Water Resources Research

RESEARCH ARTICLE
10.1029/2022WR033618

Response of Two Glaciers in Different Climate Settings of the Tibetan Plateau to Climate Change Through Year 2100 Using a Hybrid Modeling Approach

Pengfei Han[1,2], Di Long[2,3], Fanyu Zhao[2,3], and Louise J. Slater[4]

[1]School of Hydraulic Engineering, Dalian University of Technology, Dalian, China, [2]State Key Laboratory of Hydroscience and Engineering, Department of Hydraulic Engineering, Tsinghua University, Beijing, China, [3]Key Laboratory of Hydrosphere Sciences of the Ministry of Water Resources, Beijing, China, [4]School of Geography and the Environment, University of Oxford, Oxford, UK

Key Points:

- Glacier geometry projections are examined, and both the two glaciers of different types are expected almost disappear by 2100
- Glacier runoff and the timing of peak water for the Parlung No. 94 and the Dongkemadi Glacier are estimated
- Peak glacier runoff occurs later and is larger for higher emission scenarios and for the continental glacier than the maritime glacier

Supporting Information:

Supporting Information may be found in the online version of this article.

Correspondence to:

D. Long,
dlong@tsinghua.edu.cn

Citation:

Han, P., Long, D., Zhao, F., & Slater, L. J. (2023). Response of two glaciers in different climate settings of the Tibetan Plateau to climate change through year 2100 using a hybrid modeling approach. *Water Resources Research*, *59*, e2022WR033618. https://doi.org/10.1029/2022WR033618

Received 2 SEP 2022
Accepted 22 MAR 2023

Author Contributions:

Conceptualization: Pengfei Han, Di Long
Investigation: Pengfei Han
Methodology: Pengfei Han, Di Long, Fanyu Zhao
Software: Pengfei Han
Supervision: Di Long, Louise J. Slater
Validation: Pengfei Han, Fanyu Zhao
Writing – original draft: Pengfei Han
Writing – review & editing: Pengfei Han

Abstract Glaciers in High Mountain Asia (HMA) have been continuously retreating over the past four decades under global warming, affecting water availability for humans and ecosystems. However, the potential differences in mass loss and glacier runoff between maritime and continental glaciers of HMA are poorly understood. To understand the response of both types of glaciers to climate change, this study developed a hybrid modeling approach suited to data-sparse regions, and applied the proposed approach to the Parlung No. 94 Glacier (a maritime glacier) and the Dongkemadi Glacier (a continental glacier) to project glacier change under climate change. Results show that the maritime glacier has a higher balance amplitude and more negative net balance than the continental glacier. Forced by model outputs from the sixth phase of the Coupled Model Intercomparison Project, both glaciers are projected to melt almost entirely by year 2100 under the highest emission scenario (SSP585). The projected year by which the continental glacier's volume (area) is expected to halve, relative to year 2018, is about 5–11 (14) years later than that of the maritime glacier due to lower glacier retreat rates. Glacier runoff projections indicate that the peak glacier runoff occurs later and is larger for higher emission scenarios and for the continental glacier than the maritime glacier. The peak water year for the Dongkemadi Glacier is projected to occur about 24–35 years later than for the Parlung No. 94 Glacier, for which it is expected to occur by the mid-21st-century.

Plain Language Summary Glaciers over High Mountain Asia are critically important for providing freshwater resources and regulating hydrological regimes. However, they are expected to continuously retreat throughout the 21st century. Reliable projection of glacier changes is highly essential for water resource management and risk prevention. Here a temperature-index melt model coupled with a glacier dynamic model (Δh-parameterization) is developed to project response of two glaciers of different types on the Tibetan Plateau to climate change through 2100. The simulated glacier mass balances show high consistency with observations during historical period. Driven by Coupled Model Intercomparison Project Phase 6 Global Climate Models, both the two glaciers are anticipated to melt almost entirely by 2100. In addition, the Parlung No. 94 Glacier is expected to reach the peak water of glacier runoff by 2050, while peak water of the Dongkemadi Glacier will be reached 24–35 years later. The proposed approach is reliable for projecting future glacier changes and easy to apply over poorly gauged regions, given the low data demand.

1. Introduction

Glaciers play an important role as a "solid" reservoir, providing freshwater resources and regulating hydrological regimes (Biemans et al., 2019; Immerzeel et al., 2020; Li et al., 2022; Pritchard, 2019; Viviroli et al., 2007; J. Xu et al., 2009). In dry or warm seasons, when glaciers melt, the meltwater can compensate for low flow runoff (Huss & Hock, 2018). Glaciers are sensitive to environmental and climate changes, and are indicators of climate change (Haeberli & Beniston, 1998; Haeberli et al., 2002). Mountain glaciers are more sensitive to climate change due to a warmer climate and smaller scale than polar glaciers (Bach et al., 2018). With global warming, most mountain glaciers around the world are shrinking, and are expected to continue shrinking throughout the 21st century (Bamber et al., 2018; Hock et al., 2019; Marzeion et al., 2020; Zemp et al., 2015, 2019). High Mountain Asia (HMA) hosts 20.4% and 4.4% of the global area and volume of glaciers, respectively (Farinotti et al., 2019a), and glaciers in HMA have been retreating continuously over the past four decades (Bhutiyani

et al., 2010; Gardner et al., 2013; Maurer et al., 2019). In the case of a future global warming of 1.5°C, HMA is projected to have a higher warming of 2.1°C ± 0.1°C due to elevation-dependent warming (Marzeion et al., 2020; Maurer et al., 2019; Pepin et al., 2015; You et al., 2020), leading to accelerated retreat of glaciers by the end of the 21st century.

Observation and modeling of glacier mass balance from previous studies indicate that glaciers across HMA show high spatial variability in glacier mass balance change (Brun et al., 2017; Gardner et al., 2013; Yao et al., 2012; Zhao et al., 2022). The heterogeneity of glacier status is affected by many factors including glacier type (continental glacier, subcontinental and maritime), temperature rise, debris cover and other factors (Kraaijenbrink et al., 2017; Yao et al., 2012). Among these factors, the glacier type or the climate setting of a glacier are connected with glacier retreat rates and mass balance sensitivity to climate change. Glaciers in the maritime climate regime of the Nyainqentanglha region, for instance, have a large negative rate of mass loss, while glaciers in the more continental climate regime of the Karakoram and Pamir regions have a small negative rate of mass loss or even gain mass (Brun et al., 2017; Gardner et al., 2013). Maritime glaciers are more sensitive to climate change than glaciers located in continental climates (O'Neel et al., 2014; M. Xu et al., 2012). Therefore, maritime and continental glaciers may behave differently in response to future climate change in terms of glacier retreat processes and glacier runoff regimes. To understand the response of both types of glaciers to climate change, it is necessary to project future changes in glacier characteristics using glacier evolution models.

Glacier evolution can be divided into two different parts: the surface mass balance and glacier dynamics. Surface mass balance is the difference between accumulation and ablation. Glacier dynamics are associated with changes in glacier geometry (e.g., area, length, thickness, and volume) caused by changes in the glacier mass balance and glacier rheological parameters (e.g., glacier temperature and glacier bed state). Frontal ablation is also an important component of glacier mass budget for marine-terminating glaciers, which is dominated by mass loss due to calving and submarine melt. Wind effects and sliding also impact the glacier mass budget, and are particularly important over mountainous regions due to large slopes and strong wind. Historical glacier changes have been extensively investigated in previous studies with more focus on changes in glacier mass balance, and surface glacier mass balance models have been coupled with hydrological models to resolve glacier melt runoff (Gao et al., 2012; Hagg et al., 2013; Konz & Seibert, 2010; Omani et al., 2017). Glacier area changes or ice dynamics can be omitted considering that short-term glacier change is limited (Huss & Hock, 2015). Ice dynamics are an essential glacier retreat process and glacier geometry change is significant when predicting long-term glacier changes. Glacier geometry changes cannot be omitted in such a case, as the impact of changing glacier areas on hydrological fluxes such as glacier runoff can be substantial. Driven by glacier mass balance simulation, glacier dynamic models can be used to predict glacier changes in response to climate change.

For a snow and ice melt model that simulates the glacier mass balance process, temperature-index models are appropriate for the HMA region, given its scarce and fragmented glacio-meteorological records due to complex topography and inclement weather conditions. Temperature-index models generally require precipitation and temperature data as forcing inputs, but they perform well in simulating snow and glacier melting processes at daily and monthly steps (Hock, 2003; Huss & Hock, 2018) and have been applied in many studies (Chen et al., 2017; Engelhardt et al., 2013; Han et al., 2019, 2021; Nolin et al., 2010; Rahman et al., 2013; Reveillet et al., 2017). As in the case of glacier dynamic models, physically-based glacier dynamic models need a large number of glacier observations (e.g., ice thickness, glacier surface velocity, surface temperature, and glacier bedrock map) as forcing input, and the numerical simulation process is generally computationally expensive. But with the increasing availability of regional/global data sets such as glacier mass loss rates (Hugonnet et al., 2021), glacier terminus position (Kochtitzky & Copland, 2022), ice velocity (Millan et al., 2022) and ice thickness (Farinotti et al., 2019a), regional/global glacier dynamic modeling approaches have been increasingly applied in studies (Maussion et al., 2019; Wijngaard et al., 2019; Zekollari et al., 2022).

Empirical glacier evolution models solely need the surface mass balance simulation as driving data. Changes in glacier geometry under climate change can then be projected based on the empirical relationships between the glacier mass balance and glacier area (Huss & Hock, 2015; Seibert et al., 2018). Widely used empirical glacier evolution models include volume-area scaling (V-A) approaches (Bahr et al., 1997; Hock et al., 2019; Marzeion et al., 2020; Radić & Hock, 2006), accumulation area ratio (AAR) approaches (Kulkarni, 1992; Kulkarni et al., 2004; Schaefli et al., 2007), and Δh-parameterization approaches (Huss & Hock, 2018; Huss et al., 2010; Rounce et al., 2020; Seibert et al., 2018). Volume-area or volume-length scaling approaches account

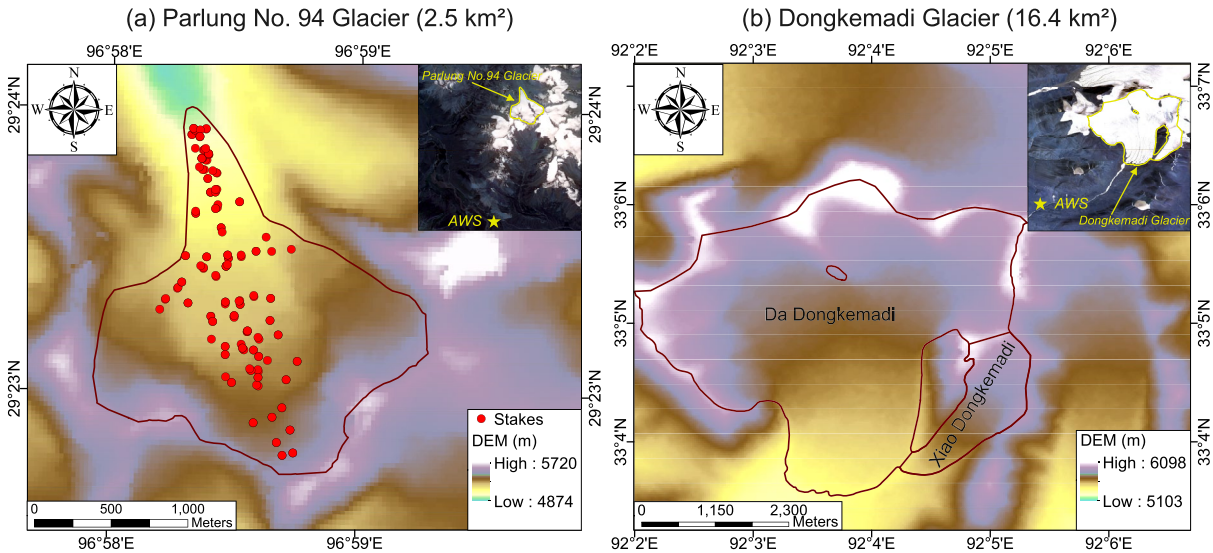

Figure 1. Locations of the Parlung No. 94 Glacier, the Dongkemadi Glacier, automatic weather stations (yellow star in the top right inset panel), and ablation stakes (red dots).

for variations in glacier length but in a simplistic fashion, and neglect changes in surface elevation (Huss & Hock, 2015). The Δh-parameterization approach requires limited glacier input data, and can describe the glacier thickness change at different elevations in response to an overall ice mass change (Huss et al., 2010). The Δh-parameterization approach has been shown to be an efficient alternative to more complex glacier dynamic models (Huss & Hock, 2015; Huss et al., 2010).

The main aim of this study was to develop a temperature-index snow and ice melt model coupled with an empirical glacier evolution model (Δh-parameterization), apply the hybrid modeling approach to glaciers in different climate settings, and improve our understanding of future evolution of different types of glaciers in response to climate change. We focus on two glaciers on the Tibetan Plateau (TP): the Parlung No. 94 Glacier, a typical maritime glacier on the southeast TP, and the Dongkemadi Glacier, a continental glacier located in the hinterland of the TP. Glacier model parameters are derived through calibration with glacier mass balance observations during the historical period (2008–2018 for the Parlung No. 94 Glacier and 1990–2010 for the Dongkemadi Glacier). The model is then forced with outputs from six bias-corrected Global Climate Models (GCMs) selected from the Coupled Model Intercomparison Project Phase 6 (CMIP6) to project changes in the area and volume of the Parlung No. 94 Glacier and the Dongkemadi Glacier until year 2100. Glacier runoff and corresponding peak water are also projected to assess the impact of glacier retreat on catchment hydrology in continental and maritime climates.

2. Study Area and Data

2.1. Study Area

We focused on two glaciers: the Parlung No. 94 Glacier (maritime glacier) and the Dongkemadi Glacier (continental glacier), which have relatively complete glacier observation records. The Parlung No. 94 Glacier is a typical valley-type glacier with an area of about 2.5 km^2 and an axis length of about 2.9 km. The glacier elevation ranges from 5,000 to 5,600 m above sea level (a.s.l.) and decreases from south to north. The study area, roughly ranging between 96°58′–97°E and 29°22′–29°24′N, is located in the southeast TP, which is influenced mostly by the southeast monsoon and hence has the longest rainy season over the TP (Yang et al., 2013). The southeast TP has about 6,000 maritime glaciers with a total area of about 9,470 km^2, caused by abundant precipitation and complex topography (Shi et al., 2008; Yang et al., 2010). There is an automatic weather station (AWS) operating in the study area, located about 7 km south of the Parlung No. 94 Glacier (96°57′E and 29°19′N, Figure 1). The AWS was set up in June 2006 with an elevation of 4,600 m a.s.l., providing precipitation, 2 m air temperature, wind speed and other meteorological observations (further information on the AWS can be found in Yang

et al. (2013)). During 2008–2018, annual precipitation at the AWS ranged from 180 to 360 mm, with mean annual precipitation of 269 mm, and annual mean air temperatures ranged from −2.3°C to −1.0°C with a mean annual temperature of −1.6°C. S. J. Wang (2018) found that the mean annual temperature of the southeast TP increased by 0.25°C per decade between 1961 and 2012. With a relatively high rate of warming, glaciers over the southeast TP are expected to retreat quickly (Yang et al., 2008). For instance, the glacierized area in the Boxoila mountain range in the southeast TP shrank by 12.7% from the 1970s to 2009 and, accordingly, the area of glacial lakes increased by 26.8% (W Wang et al., 2011).

The Dongkemadi Glacier, located in the hinterland of the TP, is a compound valley glacier formed by the south-facing Da Dongkemadi Glacier and the southwest-facing Xiao Dongkemadi Glacier. The Da Dongkemadi Glacier is the main glacier, with an area of about 14.6 km^2, an altitude range of 5,278–6,096 m, and a multi-year glacier equilibrium line of 5,600 m. The Xiao Dongkemadi Glacier is a branch glacier with an area of about 1.76 km^2, an altitude range of 5,375–5,903 m, and a multi-year glacier equilibrium line of 5,620 m. There is an AWS set in the Base Camp (BC, 5,162 m) that records precipitation and air temperatures. The Dongkemadi Glacier is a typical continental glacier with gentle slopes and little debris cover. The climate of the Dongkemadi Glacier is characterized by a cold season and a warm season. The cold season is generally from October to May in the following year, and the climate is cold and dry, affected primarily by westerly wind circulations. The warm season lasts for only 4 months from June to September, during which the climate is warm and humid due to the influence of the southwest Indian Ocean monsoon. According to AWS records, the multi-year average annual precipitation of the Dongkemadi Glacier is 600 mm, and the precipitation is mainly concentrated in the warm season (496 mm), accounting for 83% of the total precipitation.

2.2. Data

2.2.1. Meteorological Measurements

Precipitation and air temperatures are the most important forcing data for snow and ice melt modeling, and precipitation and air temperature observations from AWSs were used in this study. The AWS used a Geonor T-200B weighing bucket precipitation gauge to record the amount of precipitation, which is the collective mass of solid (snow) and liquid (rain) precipitation. Due to instrumental failure and other possible factors, data gaps inevitably exist for the precipitation and air temperature observations. Bias-corrected precipitation and air temperature from ERA5 were used to fill the data gaps and produce a consecutive precipitation and air temperature data series during 2008–2018 for the Parlung No. 94 Glacier (1990–2018 for the Dongkemadi Glacier). ERA5 is a new climate reanalysis data set from ECMWF (5th generation) with a finer spatial grid (31 km) and higher time resolution (hourly) than ERA-Interim that has a spatial and temporal resolution of 79 km and 3-hourly, respectively (Hersbach et al., 2020). Compared with precipitation records from the T-200B gauge, precipitation data in the corresponding grid cell from ERA5 showed an overestimation for both frequency and total amount, as was also confirmed by other studies (Hong et al., 2021; Jiang et al., 2021). Therefore, we used a scaling factor and occurrence threshold to adjust ERA5 precipitation data, to make it consistent with T-200B gauge precipitation records, in terms of the cumulative number of precipitation events and cumulative precipitation amount. As for air temperatures, a scaling factor and bias value were used to adjust ERA5 air temperature data.

2.2.2. CMIP6 Data

The Coupled Model Intercomparison Project is organized by the World Climate Research Programme (WCRP), and is now in its sixth phase (CMIP6). Simulation data produced by models under previous phases of CMIP have been widely used in research, and shown to be helpful for improving our understanding of climate and the influence of climate change (Cook et al., 2020; Edwards et al., 2021; Hofer et al., 2020; O'Neill et al., 2016; Tokarska et al., 2020; T. Wang et al., 2021). Here we used precipitation and air temperature data from six GCMs (i.e., CanESM5, EC-Earth3, GFDL-ESM4, MIROC6, MPI-ESM1-2-HR, and MRI-ESM2-0 with parent variant label r1i1p1f1) of three Shared Socioeconomic Pathway (SSP) scenarios (SSP126, SSP245, and SSP 585) as forcing data to project future glacier changes. And using outputs from GCMs and RCMs (Regional Climate Models) as forcing data will derives consistent results (Figure S8 in Supporting Information S2). The three SSP scenarios assume continuous rise of carbon emissions with an additional radiative forcing of 2.6, 4.5, and 8.5 W/m^2 by the year 2100, respectively. SSP126 is the optimistic scenario with green and sustainable economic growth, SSP245 represents the medium pathway of future greenhouse gas emissions, and SSP585 represents the highest warming emission scenario with strong fossil-fueled economic growth (Gidden et al., 2019).

To preserve the physical consistency between precipitation and air temperature data from CMIP6 and observations from the AWS, we applied a classic bias correction approach to adjust the precipitation and air temperature data from CMIP6. The quantile mapping (QM) algorithm (Cannon et al., 2015) was used to correct systematic distributional biases in precipitation output from CMIP6. The QM algorithm relies on the assumptions that the cumulative distribution functions (CDFs) of precipitation output from CMIP6 and precipitation observations from AWS are the same, and climate model biases to be corrected are stationary from the past to the future periods. Then the simulated future precipitation was corrected according to the CDFs of the observed and simulated precipitation in the historical period. As for air temperature, CMIP6 output was corrected by adding bias values for each month using the following equation:

$$\Delta T(m) = T_{\text{obs}}(m, y1{:}y2) - T_{\text{model}}(m, y1{:}y2) \tag{1}$$

where $\Delta T(m)$ is the bias value for month m; $T_{\text{obs}}(m, y1{:}y2)$ and $T_{\text{model}}(m, y1{:}y2)$ are the mean air temperatures from AWS's observations and CMIP6 in month m for periods $y1$ to $y2$ (year 2008–2014 in this study).

2.2.3. Ancillary Data Sets

There are five types of ancillary data sets used in this study: (a) Topographical information on the study area, that is, a digital elevation model (DEM) is extracted from NASADEM with a spatial resolution of 30 m × 30 m, which is a reprocessing of Shuttle Radar Topography Mission (SRTM) data by incorporating the best available other data; (b) Successive mass balance measurements across the entire glacier and ablation stakes, which were carried out on the Parlung No. 94 Glacier during 2008–2018 (downloaded from the world glacier monitoring service (WGMS) at https://wgms.ch/). For the Dongkemadi Glacier, there are only glacier-wide mass balance observations available from 1990 to 2010; (c) Farinotti et al. (2019a) estimated the ice thickness distribution of approximately 215,000 glaciers worldwide with glacier surface topography and five different ice dynamic models. The estimated ice thickness distribution is used as initial ice thickness distribution for the Parlung No. 94 Glacier and the Dongkemadi Glacier; (d) A glacier outline of year 2008 is provided through RGI version 6.0 (Consortium, 2017); and (e) Two RapidEye satellite images acquired on 13 September 2013 and 17 September 2018. The two satellite images have a high spatial resolution of 5 m × 5 m and were used to derive the outlines of the Parlung No. 94 Glacier in years 2013 and 2018, respectively. The GaoFen-7 (GF-7) satellite image with a high spatial resolution of 3 m × 3 m acquired on 26 February 2021 was used to derive the outlines of the Dongkemadi Glacier in 2021. Comparisons between observations and simulations for glacier outlines are provided in Figures S9–S11 in Supporting Information S2.

3. Methodology

3.1. Snow and Ice Melt Model Description

A temperature-index snow and ice melt model (TSI) was used here, driven by topographic data (elevation, aspect, and slope for the study area) and meteorological data (daily precipitation and temperature). The glacier area of the catchment is simulated with two conceptual reservoirs: glacier ice and liquid water in the glacier. Snowpack could exist on the top of the glacier and is also represented with a solid and a liquid reservoir for snow and water content, respectively. Precipitation is partitioned into solid (snow), liquid (rain), and mixed phases in terms of the air temperature and temperature thresholds.

$$P_{\text{s}} = \begin{cases} 0 & T_{\text{air}} \geq T_{\text{r}} \\ \left(\dfrac{T_{\text{air}} - T_{\text{s}}}{T_{\text{r}} - T_{\text{s}}}\right) \cdot P_{\text{tot}} & T_{\text{s}} < T_{\text{air}} < T_{\text{r}} \\ P_{\text{tot}} & T_{\text{air}} \leq T_{\text{s}} \end{cases} \tag{2}$$

where P_{s} and P_{tot} are the solid and total precipitation, respectively; T_{r} and T_{s} are the temperature thresholds for rainfall and snowfall, respectively; and T_{air} is the air temperature.

Air temperature at each grid cell is assumed to decrease linearly with elevation and determined by a constant lapse rate (dT/dz), while precipitation is interpolated with a constant precipitation gradient (dP/dz). In addition, a precipitation correction factor is needed to account for gauge under-catch errors (C_{prec}). Hence, the precipitation and air temperature are calculated as follows:

$$P_i = C_{\text{prec}} \cdot P_{\text{AWS}} \cdot (1 + (z_i - z_{\text{ref}}) \cdot dP/dz) \tag{3}$$

$$T_i = T_{\mathrm{AWS}} - (z_i - z_{\mathrm{ref}}) \cdot dT/dz) \tag{4}$$

where P_i/T_i is the interpolated precipitation/air temperature at grid cell i; $P_{\mathrm{AWS}}/T_{\mathrm{AWS}}$ is the observed precipitation/air temperature from AWS; z_i is the elevation of grid cell i; and z_{ref} is the elevation of the AWS (4,600 m).

The liquid precipitation (rainfall) is added to the water content of snow or the liquid reservoir of glaciers if there is no snowpack layer. Part of liquid water may refreeze under cold weather conditions. As for solid precipitation, the spatial variation in snow accumulation is influenced by snowdrift, avalanches, and wind redeposition. The effect of snowdrift and avalanches is taken into account by decreasing snow accumulation from 100% to 0% between a slope angle of 40°–60° (Huss et al., 2008). Wind redeposition is well indicated by curvature (Blöschl et al., 1991), and the solid precipitation is multiplied a factor that varies between 0.5 and 1.5, depending on the curvature value taken to describe the differential deposition of snow.

Temperature-index modeling of snow and ice melt has a stronger physical basis than previously assumed (Ohmura, 2001), because snow and ice melt is highly correlated with longwave heat flux, which can be well represented by air temperature. Here the snow or ice melt was calculated at every grid cell.

$$M_{\mathrm{snow/ice}} = \begin{cases} DDF_{\mathrm{snow/ice}} \cdot \left(T_{\mathrm{air}} - T_{\mathrm{snow/ice,mlt}}\right) & T_{\mathrm{air}} > T_{\mathrm{snow/ice,mlt}} \\ 0 & T_{\mathrm{air}} \le T_{\mathrm{snow/ice,mlt}} \end{cases} \tag{5}$$

where $M_{\mathrm{snow/ice}}$ is melted snow/ice; $T_{\mathrm{snow/ice,mlt}}$ is the snow/ice melting temperature threshold; and $DDF_{\mathrm{snow/ice}}$ is the degree-day factor for snow/ice.

We applied an additional topographic factor for the snow degree-day factor, so as to consider the faster and slower snowmelt due to the effects of slope and aspect. DDF_{snow} is calculated as follows:

$$DDF_{\mathrm{snow}} = DDF_{\mathrm{snow,0}} \cdot (1 - AM \cdot \sin(s) \cdot \cos(a)) \tag{6}$$

where AM is a calibrated parameter; s is slope; a is aspect; and $DDF_{\mathrm{snow,0}}$ is calculated from an application of a sinusoidal equation:

$$DDF_{\mathrm{snow,0}} = \frac{d_{\mathrm{s,mlt6}} + d_{\mathrm{s,mlt12}}}{2} + \frac{d_{\mathrm{s,mlt6}} - d_{\mathrm{s,mlt12}}}{2} \cdot \sin\left(\frac{2\pi}{365} \cdot (\mathrm{doy} - 81)\right) \tag{7}$$

where $d_{\mathrm{s,mlt6}}$ and $d_{\mathrm{s,mlt12}}$ are the maximum and minimum snowmelt factors on 21 June and 21 December, respectively, and doy is the day of the year (Fontaine et al., 2002).

Melted snow or ice is added into the liquid reservoir of snow or glaciers, and the water content exceeding snowpack water holding capacity will enter the liquid water reservoir of glaciers. If the temperature is below the temperature threshold, part of the water content in the snow layer refreezes. Therefore, the annual net glacier mass balance is calculated as follows:

$$B_{\mathrm{net}} = P_{\mathrm{s}} - M_{\mathrm{ice}} + C_{\mathrm{re}} \tag{8}$$

where B_{net} is the annual net glacier mass balance; P_{s} is the solid precipitation; M_{ice} is the ice melt; and C_{re} is the refrozen water.

3.2. Calibration of Model Parameters and Validation of Model Performance

Parameters that need to be calibrated are shown in Table 1 and we set parameter ranges following previous studies. More specifically, parameter boundaries related to melt and accumulation processes (T_{r}, T_{s}, $T_{\mathrm{snow/ice,mlt}}$, $d_{\mathrm{s,mlt6}}$, $d_{\mathrm{s,mlt12}}$, and DDF_{ice}) were determined according to Chen et al. (2017) and Han et al. (2019), parameter boundaries related to forcing data (dT/dz, dP/dz, and C_{prec}) were determined according to Hagg et al. (2013), and the range of AM was set as 0.01 to 0.98 following Stahl et al. (2008). Glacier-wide mass balance observations from in-situ measurements were used as calibration reference and validation data. We used the NSGA-II algorithm (Deb et al., 2002) for optimizing model parameters by maximizing the match between modeled and observed glacier mass balances (Eis et al., 2021; B. Marzeion et al., 2012; Schuler et al., 2007), and their calibrated values for the Parlung No. 94 Glacier and the Dongkemadi Glacier are provided in Table 1.

Table 1
Parameters of the TSI Model That Need to Be Calibrated and Their Values for the Parlung No. 94 (P) Glacier and the Dongkemadi Glacier (D) in This Study

Parameter	Description	Unit	Lower bound	Upper bound	Value for *P*	Value for *D*
T_s	Snowfall temperature threshold	°C	−4	2	−1.1	−1.0
T_r	Rainfall temperature threshold	°C	−3	3	2.9	3
$T_{snow,mlt}$	Snowmelt temperature threshold	°C	−6	3	0.2	−0.9
$d_{s,mlt6}$	Max. snowmelt factor	mm °C^{-1} d^{-1}	3	8	5.4	6.7
$d_{s,mlt12}$	Min. snowmelt factor	mm °C^{-1} d^{-1}	0	3	3	0.01
dT/dz	Temperature lapse rate	°C/km	4	8	5	6.9
dP/dz	Precipitation gradient constant	%/100 m	1	30	20	18
C_{prec}	Precipitation correction factor	–	1	2	2	1.1
AM	Influence factor of aspect/slope on snowmelt	–	0.01	0.98	0.92	0.9
$T_{ice,mlt}$	Ice melting temperature threshold	°C	−6	3	0.1	−0.8
DDF_{ice}	Degree-day factor for ice	mm °C^{-1} d^{-1}	6	10	7.4	9.7

For the Parlung No. 94 Glacier, glacier-wide mass balance observations of balance years 2013/2014 (13/14) to 2017/2018 (17/18) were used for calibration, and mass balance years from 2007/2008 (07/08) to 2012/2013 (12/13) were set as the validation period. For the Dongkemadi Glacier, glacier-wide mass balance observations are only available for the Xiao Dongkemadi Glacier. Calibration and validation periods for the Xiao Dongkemadi Glacier were set as mass balance years 1990/1991 (90/91) to 1999/2000 (99/00) and 2000/2001 (00/01) to 2009/2010 (09/10), respectively. To evaluate the performance of glacier mass balance simulation, we calculated the root-mean-square error (*RMSE*), Pearson correlation coefficient (*CC*), and mean relative bias (*Bias*) as performance metrics (Table 2).

where $Sim(i)$ is the simulated variables, $Obs(i)$ is the observed variables, $\overline{Sim}$ is the mean of the simulations, and $\overline{Obs}$ is the mean of the observations.

3.3. Δ*h*-Parameterization

To predict the dynamic response of glacier geometry to climate change, we need to translate glacier mass changes into area changes. We applied an empirical glacier dynamic model (Δ*h*-parameterization method) for glacier geometry simulation (Huss et al., 2010; Seibert et al., 2018). The Δ*h*-parameterization approach incorporates a single-valued relationship between the glacier mass and glacier area. Then glacier area changes can be calculated based on the relationship and the glacier mass balance changes from the TSI model. Specifically, we need to compute how glacier area changes with a given glacier mass balance change based on an initial glacier area and glacier ice thickness values with elevation (termed "initial glacier profile"; in the following, glacier area from RGI 6.0 and ice thickness from Farinotti et al. (2019a) are used as the initial glacier profile). The calculated glacier area changes with corresponding glacier mass balance changes are then recorded to produce a lookup table (Seibert et al., 2018). To ensure smooth changes, the calculations here are applied elevation bands with a

Table 2
Performance Metrics Used in Evaluating the Simulated Variables Against Observations

Statistic metrics	Equation	Perfect value
Root-mean-square error (*RMSE*)	$RMSE = \sqrt{\frac{\sum_{i=1}^{n}(Sim(i)-Obs(i))^2}{n}}$	0
Pearson correlation coefficient (*CC*)	$CC = \frac{\sum_{i=1}^{n}\left(Obs(i)-\overline{Obs}\right)\left(Sim(i)-\overline{Sim}\right)}{\sqrt{\sum_{i=1}^{n}\left(Obs(i)-\overline{Obs}\right)^2}\sqrt{\sum_{i=1}^{n}\left(Sim(i)-\overline{Sim}\right)^2}}$	1
Mean relative bias (*Bias*)	$Bias = \frac{\sum_{i=1}^{n}Sim(i)-\sum_{i=1}^{n}Obs(i)}{\sum_{i=1}^{n}Obs(i)}$	0

resolution of 5 m. First, the initial total glacier mass (M_{ini}, in kg) is calculated from the initial glacier profile, that is, glacier area and ice thickness in year 2008:

$$M_{\text{ini}} = \rho_{\text{ice}} \cdot \sum_{i=1}^{N} a_i \cdot h_i \tag{9}$$

where a_i and h_i are glacier area (in m^2) and glacier ice thickness (in m) for each elevation band i; and ρ_{ice} is the ice density (850 kg/m^3). Then the glacier is melted in steps of ΔM (1% of the initial total glacier mass in this study) to generate the lookup table. For the glacier melting process, we selected one of three parameterizations suggested by Huss et al. (2010) to calculate the normalized ice thickness change (Δh_i, dimensionless) for each elevation band:

$$\Delta h_i = (E_{i,\text{norm}} + a)^{\gamma} + b(E_{i,\text{norm}} + a) + c \tag{10}$$

where a, b, c, and γ are empirical coefficients and their values are −0.3, 0.6, 0.09, and 2, considering that the Parlung No. 94 Glacier is a small glacier (glacier area is about 2.6 km^2 < 5 km^2); and $E_{i,\text{norm}}$ is the normalized elevation for each elevation band i, which is computed from the maximum and minimum elevations of the glacier (E_{max} and E_{min}), and the corresponding absolute elevation (E_i):

$$E_{i,\text{norm}} = \frac{E_{\text{max}} - E_i}{E_{\text{max}} - E_{\text{min}}} \tag{11}$$

Next, the scaling factor (f_s, in m) that scales the magnitude of the dimensionless normalized ice thickness change is calculated:

$$f_s = \frac{\Delta M}{\rho_{\text{ice}} \cdot \sum_{i=1}^{N} a_i \cdot \Delta h_i} \tag{12}$$

Then, the ice thickness of elevation band i is updated as follows:

$$h_{i,k+1} = h_{i,k} + f_s \Delta h_i \tag{13}$$

where $h_{i,k}$ and $h_{i,k+1}$ are the ice thickness of elevation band i after reducing the glacier mass k and $k+1$ times by ΔM.

After the ice thickness of each elevation band is updated, the glacier area for each elevation band also needs to be updated, so as to take the area reduction into account. Here the relationship between the glacier width and glacier thickness proposed by Bahr et al. (1997) is applied to scale the glacier area of each elevation band:

$$a_{i,\text{scaled}} = a_{i,\text{initial}} \cdot \sqrt{h_i / h_{i,\text{initial}}} \tag{14}$$

where $a_{i,\text{scaled}}$ and $a_{i,\text{initial}}$ are scaled and initial glacier areas for elevation band i; and h_i and $h_{i,\text{initial}}$ are updated and initial ice thickness for elevation band i.

As the glacier is melted from steps of 0%–100% of the initial glacier mass, the lookup table recording corresponding glacier area and ice thickness for each elevation band is created. The use of a lookup table to represent the mass–area relationship allows for the inclusion of advancing glaciers. Finally, in the actual simulation of changes in glacier geometry, the glacier extent is updated at the beginning of each mass balance year (1 September). The TSI model provides the glacier mass balance change, and corresponding glacier area and ice thickness for each elevation bands are extracted from the lookup table to update glacier geometry. Therefore, by coupling the empirical glacier dynamic model (Δh-parameterization) with the TSI model (TSI-Δh model), the TSI-Δh model is able to predict the glacier's dynamic response to future climate change (Figure 2).

3.4. Glacier Runoff

Following Rounce et al. (2020), the glacier runoff, Q, is defined as all water that leaves the initial glacierized area, and is computed as follows:

$$Q = p_{\text{liquid}} + \text{ablation} - \text{refreezing} \tag{15}$$

where Q is referred to as "fixed-gauge" glacier runoff since it is equivalent to the runoff that would be measured at a virtual fixed-gauge station at the initial glacier terminus. The "fixed-gauge" glacier runoff can be divided

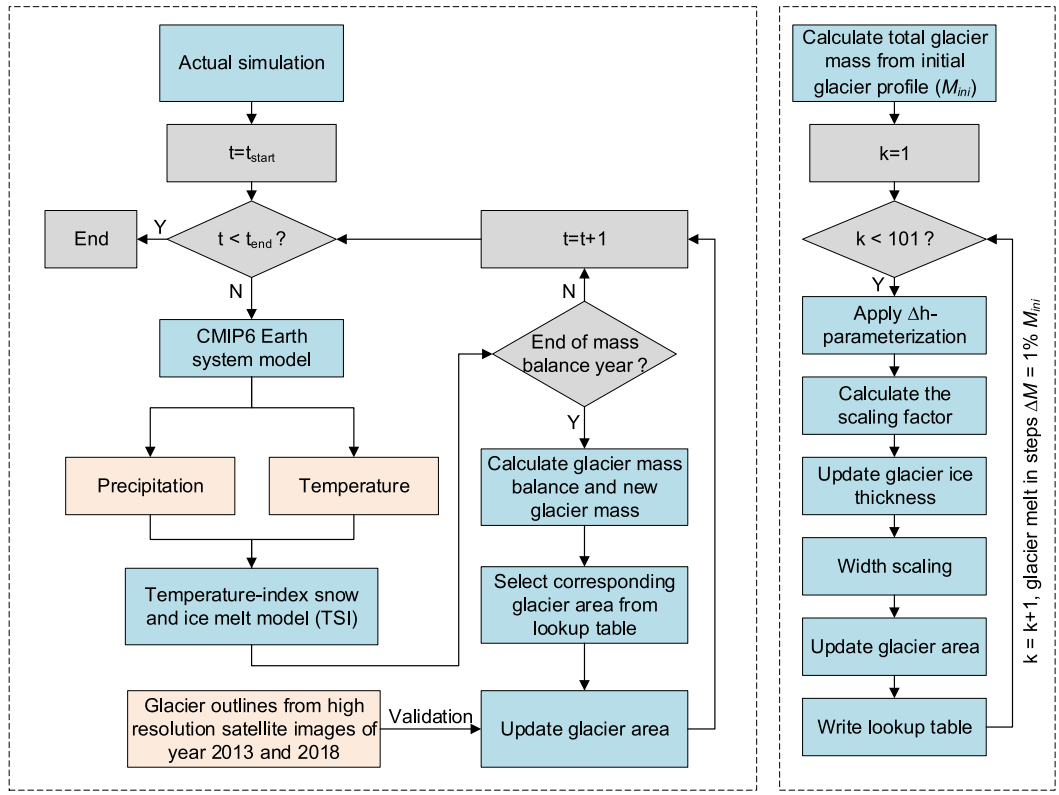

Figure 2. Flowchart of the TSI-Δ*h* model describing the response of glacier areas to glacier mass changes.

into two parts: (a) runoff from the changing glacierized area, referred to as "moving-gauge" glacier runoff, which equals runoff that would be measured at a virtual gauging station that moves with changing glacier terminus and (b) runoff from the ice-free area that was initially ice-covered, and is referred to as "off-glacier" runoff. The off-glacier runoff is computed as the sum of rain, seasonal snow melt, and refreezing from the non-glacierized portion of the initial glacier area.

4. Results

4.1. Performance of Glacier Mass Balance Simulation

Time series of simulated glacier mass balance for the Parlung No. 94 Glacier and the Dongkemadi Glacier are shown in Figure 3, and Table 3 shows corresponding performance metrics. With the calibrated parameter set using the NSGA-II algorithm, the TSI model performs well and simulated glacier mass balances are consistent with observations. For the Parlung No. 94 Glacier, modeled and measured results are very close during the calibration period, with a *CC* value of up to 0.99, an *RMSE* value of only 0.03 m w.e., and a *Bias* value of 0.02. The model performance degrades to some extent during the validation period, but it is still acceptable for the entire period given the relatively good performance metrics with an *RMSE* value of about 0.39 m w.e., *CC* value of 0.71, and *Bias* value of about −0.12. The performance degradation during the validation period is caused mostly by the poor performance in balance year 2011/2012, which shows large overestimation. According to the comparison of glacier mass balance simulation and forcing data (mean summer air temperature and mean winter precipitation, referring to Figure S1 in Supporting Information S2), winter precipitation in balance year 2011/2012 was abnormally high, given that Southwest China experienced a severe drought in 2011–2012 (Tang et al., 2014), resulting in more accumulation and therefore overestimation of glacier mass balance.

For the Dongkemadi Glacier, results show that simulated glacier mass balance changes are consistent with observations. Performance metrics in Table 3 also indicate that the simulation performs well with *RMSE* values of about 0.22 m w.e. and *CC* values higher than 0.8 during all time periods. The *Bias* value is merely 0.02 during

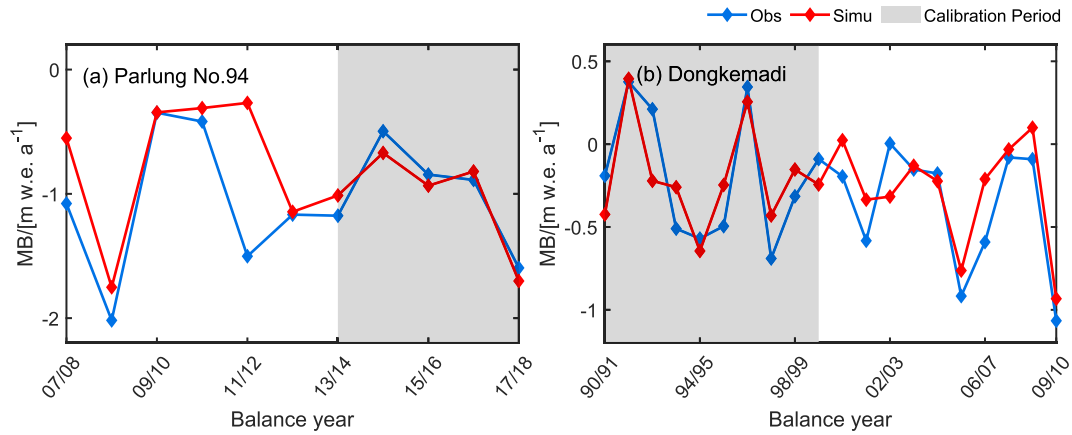

Figure 3. Temporal evolution of the annual net mass balance for (a) the Parlung No. 94 Glacier and (b) the Dongkemadi Glacier. Gray shaded areas indicate calibration periods.

the calibration period, but decreases to −0.27 due to underestimation during the validation period. In addition, observations show that the Xiao Dongkemadi Glacier experienced positively mass balanced years of 91/92, 92/93 and 96/97, which are accurately captured by the model simulation except for 92/93 mass balance year. Furthermore, consistent with previous studies (Pu et al., 2008), the glacier mass balance of the Xiao Dongkemadi Glacier has changed from significant positive equilibrium to negative since 1993, and the rate of glacier retreat shows an accelerating trend.

As shown in Braithwaite and Hughes (2020), the balance amplitude tends to be large for maritime glaciers with warm/wet climates, in which both accumulation and ablation are large, and glaciers are likely to have large net balances. In contrast, continental glaciers with cold/dry climates tend to have a low balance amplitude, in which accumulation and ablation are small, and net balances are likely to be small (negative or positive). Glacier mass balance changes over the two glaciers with different climate settings are in accordance with previous research. The continental glacier (Xiao Dongkemadi Glacier) has a lower balance amplitude than the maritime glacier (the Parlung No. 94 Glacier), and the multi-year average net balance rate is −289 mm w.e. a^{-1} with some positively balanced years. The Parlung No. 94 Glacier has a larger net balance with a multi-year average net balance rate of −1,048 mm w.e. a^{-1}, and the glacier is continuously retreating.

To further investigate the performance of simulated glacier mass balance and parameter uncertainty, we performed for each glacier a Monte Carlo run of 10,000 random parameter sets with boundaries shown in Table 1 (M. Engelhardt et al., 2014; Kuczera & Parent, 1998). The 100 best runs with the lowest *RMSEs* were selected and compared with the best model run optimized by the NSGA-II algorithm (referring to Text S1 in Supporting Information S1 and Figures S2–S5 in Supporting Information S2), indicating that simulation results with the NSGA-II calibration scheme are accurate and reliable.

Table 3
Performance Metrics for the Glacier Mass Balance Simulation of the Parlung No. 94 Glacier and the Dongkemadi Glacier

	Parlung No. 94			Dongkemadi		
	RMSE	*CC*	*Bias*	*RMSE*	*CC*	*Bias*
Calibration period	0.03	0.99	0.02	0.22	0.80	0.02
Validation period	0.53	0.66	−0.23	0.21	0.86	−0.27
Whole period	0.39	0.71	−0.12	0.22	0.83	−0.17

Note. Unit for *RMSE* is m w.e., *CC* and *Bias* are dimensionless. *RMSE*, root-mean-square error; *CC*, Pearson correlation coefficient; *Bias*, mean relative bias.

4.2. Projection of Glacier Retreat Based on CMIP6 Output

Using precipitation and temperatures from six CMIP6 GCMs under three different SSPs as forcing data, the TSI-Δ*h* model can generate the dynamic response of the glacier geometry under future climate change. Figure 4 shows time series of multi-GCM means of bias adjusted temperature and precipitation changes relative to the mean from 2008 to 2018. For the Parlung No. 94 Glacier and the Dongkemadi Glacier, the temperature under the SSP126 scenario is projected to increase by ~1.3°C and 1.8°C, respectively, by the mid-21st-century relative to the 2008–2018 mean, and then stabilize. SSP245 projects a relatively steady temperature increase of ~2.8°C and 3.2°C by 2100 for the two glaciers. SSP585 projects a constant increase in temperature throughout the century such that temperatures of the Parlung No. 94 Glacier and the Dongkemadi Glacier are projected to increase by ~5.6°C and 6.3°C

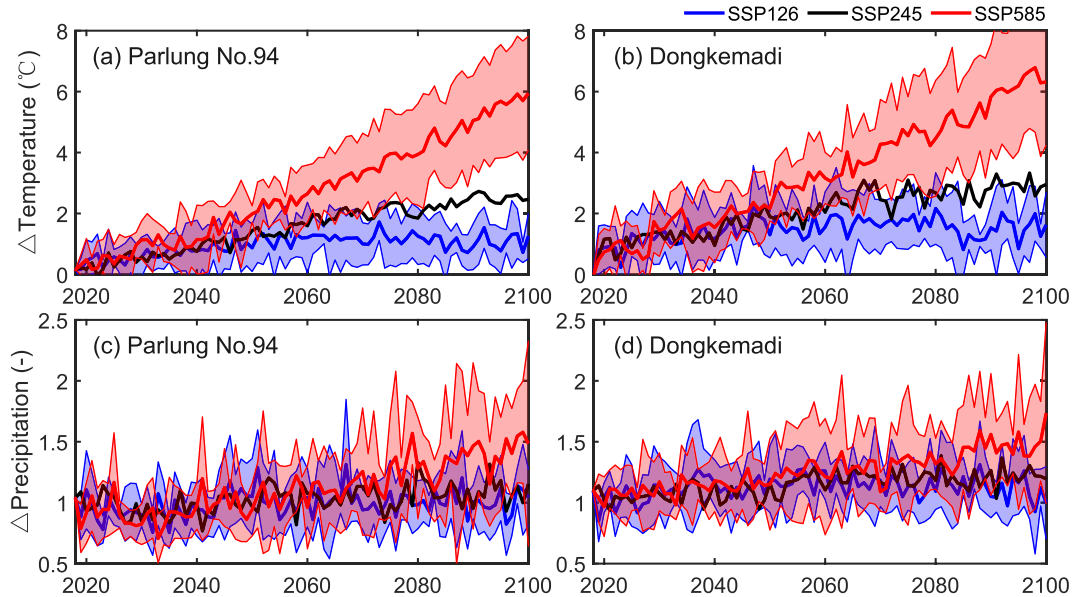

Figure 4. Multi-Global Climate Model means (±1 standard deviation) of bias adjusted temperatures (a, b) and precipitation (c, d) changes, relative to the mean from 2008 to 2018 for the Parlung No. 94 Glacier (a, c) and the Dongkemadi Glacier (b, d) from 2018 to 2100. Uncertainty is only shown for SSP126 and SSP585 for clarity.

by 2100. Precipitation changes are more variable, and the precipitation increase is largest under the SSP585 scenario, which is projected to increase by ~42% and 48% relative to the 2008–2018 mean.

Figure 5 shows changes in glacier area and volume for the Parlung No. 94 Glacier and the Dongkemadi Glacier under three SSPs from years 2018–2100. Spatial distribution projections of future ice thickness are shown in Figures S12–S13 in Supporting Information S2. Projections indicate that from 2018 to 2100, the Parlung No. 94 Glacier may experience a mass loss of 80% ± 14% (SSP126), 88% ± 8% (SSP245), and 98% ± 3% (SSP585) relative to 2018, and the Dongkemadi Glacier may experience a mass loss of 75% ± 23% (SSP126), 88% ± 12%

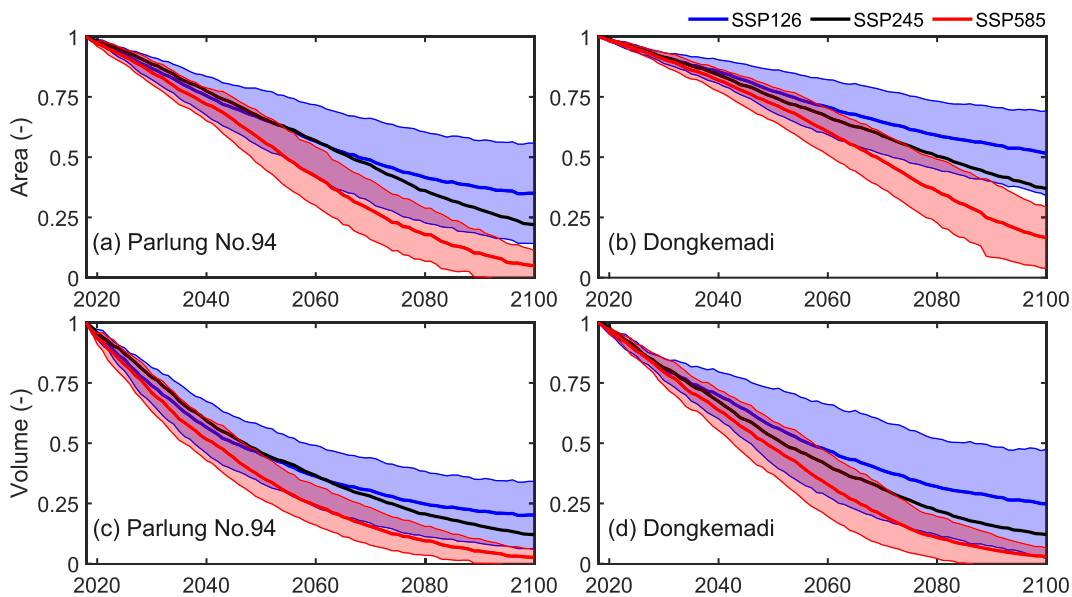

Figure 5. Multi-Global Climate Model means (±1 standard deviation) of normalized glacier area (a, b) and glacier volume (c, d) remaining, relative to 2018, from 2018 to 2100 for the Parlung No. 94 Glacier (a, c) and the Dongkemadi Glacier (b, d). Uncertainty is only shown for SSP126 and SSP585 for clarity.

Table 4
Projected Years for the Glacier Areas of the Parlung No. 94 Glacier and the Dongkemadi Glacier Decreasing to Half of the Area Measured in 2018, and Remaining Glacier Area in 2100 Under the Three SSPs (SSP126, SSP245, and SSP585)

	Parlung No. 94 Glacier			Dongkemadi Glacier		
Scenario	Year	Area/ (km^2)	Percent/(%)	Year	Area/ (km^2)	Percent/ (%)
SSP126	2018	2.37	100	2018	15.39	100
	2068	1.18	50	–	–	–
	2100	0.83	35	2100	7.94	52
SSP245	2066	1.19	50	2081	7.69	50
	2100	0.52	22	2100	5.68	37
SSP585	2055	1.16	49	2069	7.69	50
	2100	0.12	5	2100	2.55	17

(SSP245), and 97% ± 4% (SSP585). As expected, the mass loss by 2100 increases for higher emission scenarios. Compared with the Parlung No. 94 Glacier, glacier retreat rates for the Dongkemadi Glacier are relatively low, especially at the early stage of glacier retreat. These findings further indicate that the continental glacier (Dongkemadi) is likely to have smaller mass balance change rates than the maritime glacier (Parlung No. 94).

Table 4 shows the projected years by when the areas of the Parlung No. 94 Glacier and the Dongkemadi Glacier are likely to have decreased to half of the area measured in 2018, and the projections of remaining glacier areas by 2100 under the three SSPs scenarios. Table 5 shows results for glacier volume. Compared with the state of the Parlung No. 94 Glacier in 2018 (i.e., glacier area was about 2.37 km^2 and glacier volume was about 0.133 km^3), the projected years for glacier area halving under SSP126 and SSP245 are pretty close, namely 2068 and 2066, respectively. In other words, the rates of retreat are similar, due to a similar temperature increase for SSP126 and SSP245 by the mid-21st-century (Figure 4). Under the SSP585 scenario, the Parlung No. 94 Glacier is likely to halve its 2018 glacier area by 2055, and shrink to 0.12 km^2 by the end of this century, which is merely 5% of the area estimated in 2018.

For the Parlung No. 94 Glacier, projected years for the glacier volume halving under SSP126 and SSP245 are also close, namely about 2046, and the glacier volume will halve by 2041 under SSP585 (Table 5). Hence, corresponding years when the glacier volume of the Parlung No. 94 Glacier is projected to halve, relative to 2018, are 14–23 years earlier than the years estimated for glacier area, and this is related to the glacier retreat process. At the early stage of glacier melting for the Parlung No. 94 Glacier, glacier change is dominated by thinning processes due to the thick ice in ice tongue areas. As the ice thickness decreases, the glacier volume will decrease rapidly, but the glacier area may decrease more slowly as the thick ice has not melted completely. Hence, the rate of glacier area reduction is much smaller than the rate of glacier volume reduction, and the corresponding year for the glacier volume decreasing to 50% is earlier than that of glacier area. Overall, the Parlung No. 94 Glacier is expected to recede continuously even under the most optimistic climate scenario (SSP126), and it to melt almost entirely by 2100 under the worst climate scenario (SSP585).

As for the Dongkemadi Glacier, the glacier retreat rate is slower than that of the Parlung No. 94 Glacier. Compared with the glacier state in 2018 (i.e., the glacier area was about 15.39 km^2 and glacier volume was about 1.146 km^3), the glacier area of the Dongkemadi Glacier is projected to reduce to 52% by 2100 under the SSP126 scenario. Corresponding years for the glacier area halving relative to 2018 under the SSP245 and SSP585 scenarios are 2081 and 2069, respectively, which is about 14 years later than for the Parlung No. 94 Glacier. For the Dongkemadi Glacier, corresponding years for the glacier volume halving relative to 2018 under three SSP scenarios are 5–11 years later than for the Parlung No. 94 Glacier.

Table 5
Projected Years for Volumes of the Parlung No. 94 Glacier and the Dongkemadi Glacier Decreasing to Half of the Volume Measured in 2018, and Remaining Glacier Volumes in 2100 Under the Three SSPs (SSP126, SSP245, and SSP585)

	Parlung No. 94 Glacier			Dongkemadi Glacier		
Scenario	Year	Volume/ (km^3)	Percent/ (%)	Year	Volume/ (km^3)	Percent/ (%)
SSP126	2018	0.133	100	2018	1.146	100
	2045	0.067	50	2056	0.577	50
	2100	0.027	20	2100	0.284	25
SSP245	2047	0.067	50	2052	0.568	50
	2100	0.016	12	2100	0.139	12
SSP585	2041	0.067	50	2049	0.566	49
	2100	0.003	2	2100	0.034	3

Similar to the retreat process of the Parlung No. 94 Glacier, the glacier change of the Dongkemadi Glacier is also dominated by thinning processes at the early stage of the glacier melting. Hence, corresponding years when the glacier volume of the Dongkemadi Glacier decreasing to a half are 20–29 years earlier than that of glacier area. This lead time of the Dongkemadi Glacier is longer than that of the Parlung No. 94 Glacier, which is related to the dominating duration of thinning in the glacier melting process and is further discussed in Text S2 in Supporting Information S1 and Figure S6 in Supporting Information S2.

4.3. Projection of Glacier Runoff Based on CMIP6 Output

Glacier runoff reflects the volume change of glaciers, and is affected by a combination of glacier area and glacier mass balance. As glaciers recede,

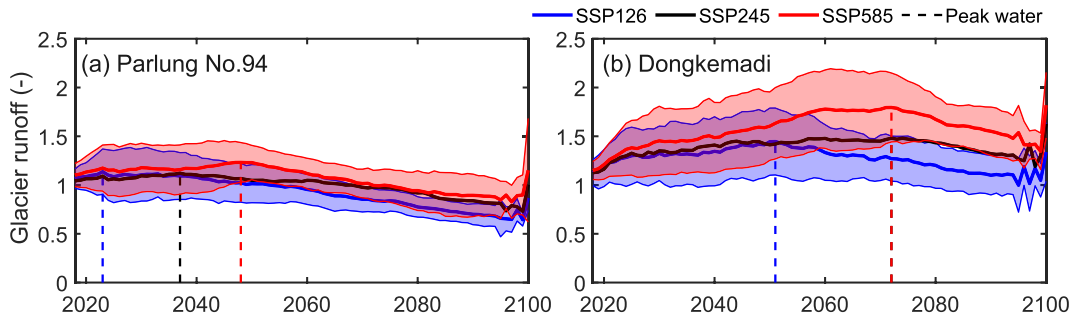

Figure 6. Time series of multi-Global Climate Model means (±1 standard deviation) of annual fixed-gauge glacier runoff (i.e., the runoff from the initially glacierized area for the Parlung No. 94 Glacier (a) and the Dongkemadi Glacier (b) for each Shared Socioeconomic Pathway (SSP) scenario from 2018 to 2100), relative to the mean annual fixed-gauge glacier runoff from 2008 to 2018. Uncertainty is only shown for SSP126 and SSP585 for clarity. Dashed lines show peak water for each SSP scenario.

water is released from long-term glacial storage. Annual glacier runoff typically increases until reaching a maximum, often referred to as "peak water." Then the runoff decreases because the reduced glacier area cannot support rising meltwater volumes anymore. Figure 6 shows time series of multi-GCM mean of annual fixed-gauge glacier runoff for the Parlung No. 94 Glacier and the Dongkemadi Glacier under the three SSPs scenarios from 2018 to 2100, relative to the mean annual glacier runoff from 2008 to 2018. From the projected time series of annual glacier runoff, peak water was calculated based on 11-year moving averages following Huss and Hock (2018). Projections of fixed-gauge annual glacier runoff indicate that peak water of the Parlung No. 94 Glacier is likely to be reached by 2023, 2037, and 2048 under the three SSPs scenarios, followed by declining glacier runoff. As for the Dongkemadi Glacier, peak water years under three SSPs scenarios are 2051, 2072, and 2072, respectively. The early peak water timing of the Parlung No. 94 Glacier indicates that it has already been experiencing a high mass loss rate since 2000, while the Dongkemadi Glacier is at the early stage of glacier retreat (Shean et al., 2020). On the other hand, the Dongkemadi Glacier is a continental glacier with a low mass loss rate, and the peak water year is much later than that of the Parlung No. 94 Glacier.

Figure 6 also indicates that the continental glacier (the Dongkemadi Glacier) produces larger peak glacier runoff than the maritime glacier (the Parlung No. 94 Glacier). Increases in annual glacier runoff for the Dongkemadi Glacier when peak water occurs can be substantial, that is, +48% (SSP126), +52% (SSP245), and +84% (SSP585) of the initial glacier runoff. However, increases in glacier runoff for the Parlung No. 94 Glacier are relatively small in comparison, as the glacier runoff increases by 12%–23% under the three SSPs scenarios. Relative increases in glacier runoff tend to be more pronounced for higher emission scenarios, which is consistent with previous studies (Huss & Hock, 2018; Rounce et al., 2020). Under lower emission scenarios, it is likely that glaciers will reach a new equilibrium more easily, so the glacial runoff will reach a peak earlier in this century. But under higher emission scenarios, in contrast, increased glacier melting caused by higher temperatures will result in larger glacier runoff and delay the peak water years.

Figure 7 shows components of fixed-gauge glacier runoff for the Parlung No. 94 Glacier and the Dongkemadi Glacier under three scenarios. Results indicate that the timing of peak water is controlled mostly by glacier meltwater, which is the largest contributor of fixed-gauge glacier runoff. For the Parlung No. 94 Glacier, multi-year mean glacier melt from 2018 to 2100 accounts for ~62% of fixed-gauge glacier runoff in SSP585, and the contribution is even larger for earlier years and lower emission scenarios. As for the Dongkemadi Glacier, multi-year mean glacier melt from 2018 to 2100 accounts for ~67% of fixed-gauge glacier runoff in SSP585. The starting point of the sharp decrease in glacier melt is later for higher emission scenarios due to higher temperatures and increased glacier melting. This timing is also later for the Dongkemadi Glacier than the Parlung No. 94 Glacier due to the continental glacier's lower rate of mass balance change. Therefore, the peak water year is later for higher emission scenarios and for continental glaciers than maritime glaciers. As for the magnitude of peak glacier runoff, it is related to glacier melt together with precipitation. Precipitation of the two glaciers shows an increasing trend from 2018 to 2100, and is particularly obvious in SSP585 (Figure 4). With later timing of peak water, the amount of precipitation is expected to be larger and contribute more to the glacier runoff. Therefore, the peak glacier runoff is also larger for higher emission scenarios and for continental glaciers than maritime glaciers.

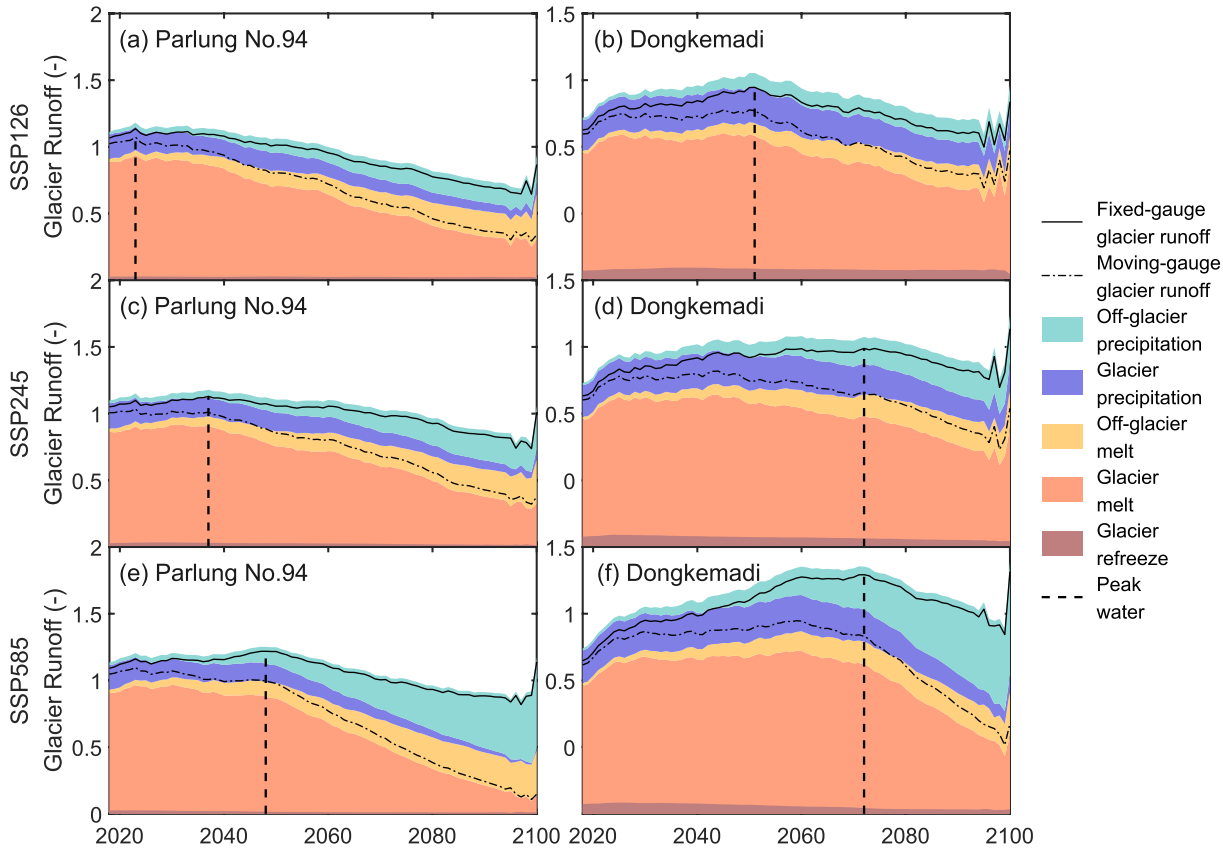

Figure 7. Multi-Global Climate Model mean of annual fixed-gauge glacier runoff and various components for the Parlung No. 94 Glacier (a, c, and e) and the Dongkemadi Glacier (b, d, and f) under the SSP126 (a, b), SSP245 (c, d) and SSP585 (e, f) scenarios from 2018 to 2100, relative to the mean annual fixed-gauge glacier runoff from 2008 to 2018.

As glaciers retreat, glacier melt will decrease and the extent of ice-free areas that were initially ice-covered will increase. Hence, the two components, that is, off-glacier precipitation and off-glacier melt, which are generated from ice-free areas are expected to become increasingly important components of fixed-gauge glacier runoff. However, the ratios of off-glacier precipitation to off-glacier melt for the Parlung No. 94 Glacier and the Dongkemadi Glacier are different (1.37 and 1.87, respectively, for multi-year mean from 2018 to 2100), which is related to glaciers' climate conditions. The Parlung No. 94 Glacier is a maritime glacier which can receive much precipitation as snow, and the amount of off-glacier (seasonal snow) melt is relatively large. Precipitation of the Dongkemadi Glacier is mainly concentrated in the warm season, and the amount of seasonal snow on ice-free areas is limited compared with liquid precipitation during summer monsoon. Figure 7 also shows the difference between fixed-gauge glacier runoff (black line) and moving-gauge glacier runoff (black dashed line) that excludes off-glacier runoff (Bliss et al., 2014). Compared with the fixed-gauge glacier runoff, using moving-gauge glacier runoff is likely to substantially underestimate the timing and amount of peak water for both glaciers. Therefore, taking fixed-gauge glacier runoff as glacier runoff seems more reasonable, and it also has greater utility for water resource managers and people who live downstream from glaciers.

Figure 8 shows relative components of fixed-gauge glacier runoff for each month at the end of the century (2090–2100) for the Parlung No. 94 Glacier and the Dongkemadi Glacier, relative to monthly runoff from 2008 to 2018 under three scenarios. The Parlung No. 94 Glacier is projected to experience significant reductions in fixed-gauge monthly glacier runoff (about −38%, −35%, and −27% for the SSP126, SSP245, and SSP585 scenarios, respectively). Peak month shows an advancing trend, advancing from August in the historical period to July for SSP126, and even to June for SSP245 and SSP585. The reason for this change is that the maritime glacier is largely influenced by the southeast monsoon, and off-glacier (seasonal snow) melt together with precipitation are expected to become increasingly important components of fixed-gauge glacier runoff as glaciers retreat. Glacier melt contributes merely ∼9% in June for the Parlung No. 94 Glacier under SSP585, while precipitation

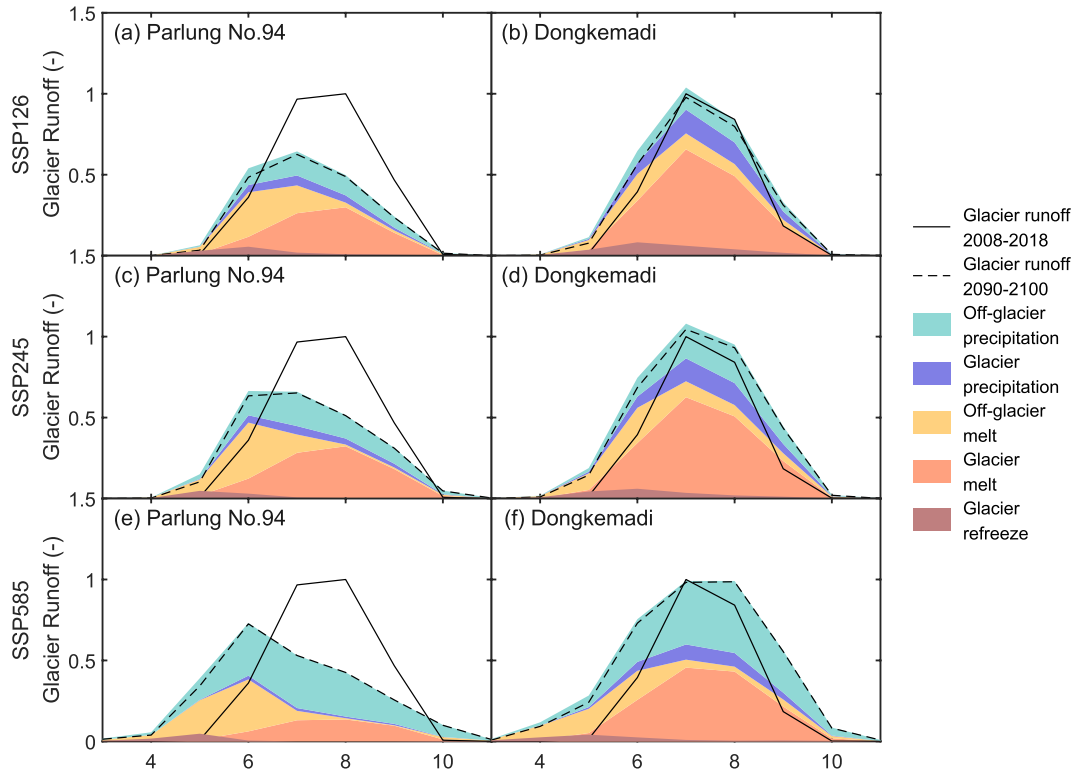

Figure 8. Mean monthly fixed-gauge glacier runoff averaged over 2008–2018 and 2090–2100 for the Parlung No. 94 Glacier (a, c, and e) and the Dongkemadi Glacier (b, d, and f) under the SSP126 (a, b), SSP245 (c, d) and SSP585 (e, f) scenarios. Runoff for both periods is normalized relative to the maximum monthly runoff from 2008 to 2018. Relative contributions from various components are shown for the runoff from 2090 to 2100.

and seasonal snow melt contribute ~47% and 44%, respectively. As a maritime glacier, a large amount of precipitation of the Parlung No. 94 Glacier falls as snowfall in winter months, and earlier timing of snowmelt leads to the advance of the peak glacier runoff month. As for the Dongkemadi Glacier, the peak of fixed-gauge monthly glacier runoff is projected to change slightly (about −2% to −5% for three scenarios), due to increasing precipitation (contributes ~22% of fixed-gauge glacier runoff in the historical period while ~54% in SSP585) despite glacier melt decreases. The peak month for the Dongkemadi Glacier is not expected to change, because most of the precipitation and melting of this accumulation glacier occurs in the summer (Liang et al., 2018).

5. Discussion

5.1. Relationship Between Glacier Retreat Rates and Forcing Data From CMIP6

To explore the relationship between glacier retreat rates and forcing data from CMIP6, we compared changes in glacier area and volume estimated with the different bias-corrected GCM outputs as forcing data (Figure 9). Changes in glacier area and volume are quite variable when using different GCM outputs under any SSP scenario. The glacier area and volume decrease at the highest rate when using MRI-ESM2-0 model outputs, followed by the CanESM5, EC-Earth3, and GFDL-ESM4 models. Both the MIROC6 and MPI-ESM1-2-HR models correspond to the lowest glacier retreat rate.

Figure 10 shows boxplots of total precipitation during winter (i.e., December–February in the following year) and mean air temperature during summer (i.e., June–August) over the 2018–2100 period from six GCMs under three SSP scenarios. Total precipitation during winter was selected for its direct relationship with glacier accumulation, whereas mean air temperature during summer is related to glacier ablation. Total winter precipitation has no obvious differences under the three scenarios, whereas mean summer air temperature has a higher value under the SSP585 scenario. Furthermore, the variation range of mean summer air temperature is larger under the SSP585 scenario than the SSP126 scenario. By comparing the projections of total winter precipitation and mean

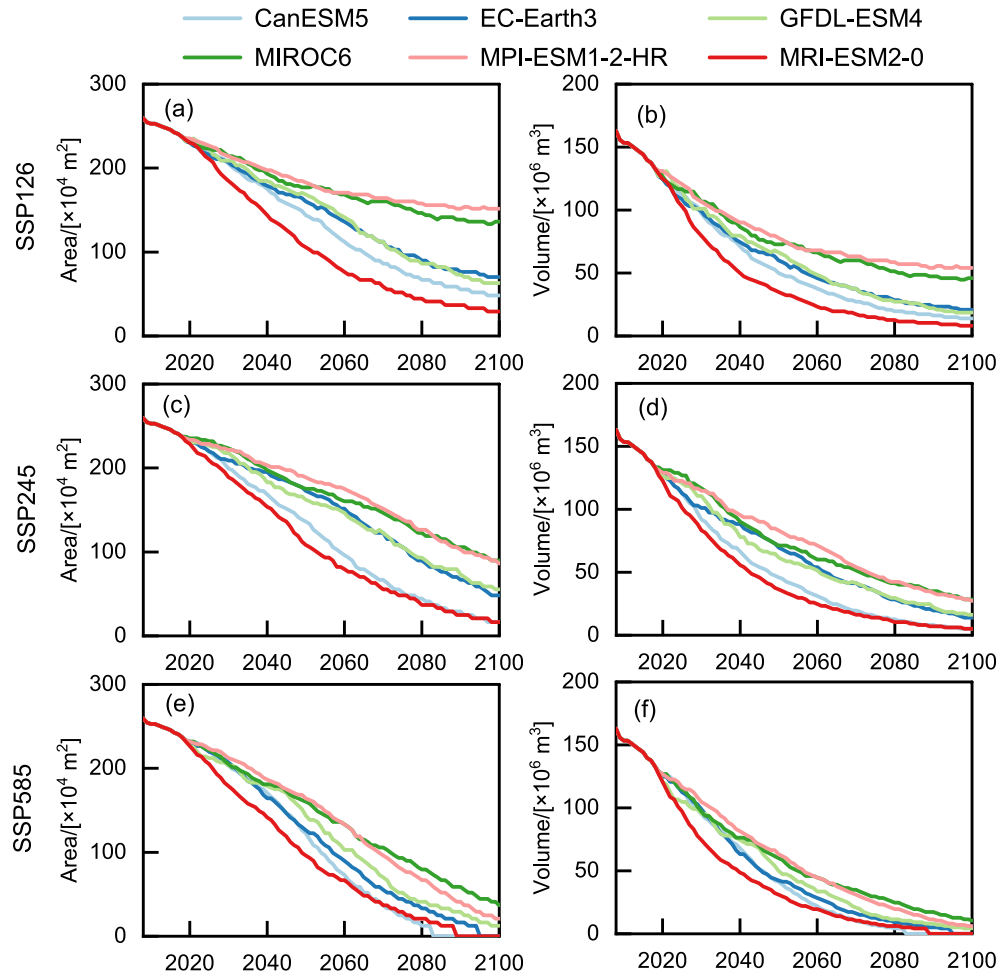

Figure 9. Changes in glacier area (left column) and volume (right column) for the Parlung No. 94 Glacier with outputs from six Global Climate Models as forcing data under three Shared Socioeconomic Pathway scenarios from 2008 to 2100.

summer air temperatures from GCMs outputs with changes in corresponding glacier areas and volume, a distinct relationship between the mean summer air temperature and the glacier retreat rate is found, which is consistent with previous studies (Sagredo et al., 2014; Vuille et al., 2008).

Mean summer air temperatures from the MRI-ESM2-0 model are higher than other models under all three SSP scenarios, and both the MIROC6 and MPI-ESM1-2-HR models have the lowest air temperatures. Hence, the glacier retreat rate from the MRI-ESM2-0 model is highest. Furthermore, the mean summer air temperature under the SSP585 scenario is about 1.4°C higher than the temperature under the SSP126 scenario, resulting in higher glacier retreat rates. As for total winter precipitation, no obvious relationship with the glacier retreat rate was found. Overall, glacier retreat rates respond more to summer air temperatures than winter precipitation, because the magnitude and importance of glacier ablation is larger than glacier accumulation if the glacier is in a retreating state.

5.2. Comparison With Previous Studies

Few studies have focused on the Parlung No. 94 Glacier and the Dongkemadi Glacier; thus, we compare our glacier projection results with regional-scale glacier projections from previous studies. This comparison might not be rigorous because neighboring glaciers can show significantly different mass balances despite a similar regional climate (Moholdt et al., 2010; Zhao et al., 2022), but it provides insights into changes in these two glaciers in the future.

For the Parlung No. 94 Glacier located in the southeast TP, comparisons can be made with regional glacier projections for South East Asia in Hock et al. (2019) and Marzeion et al. (2020) or a more specific region of the

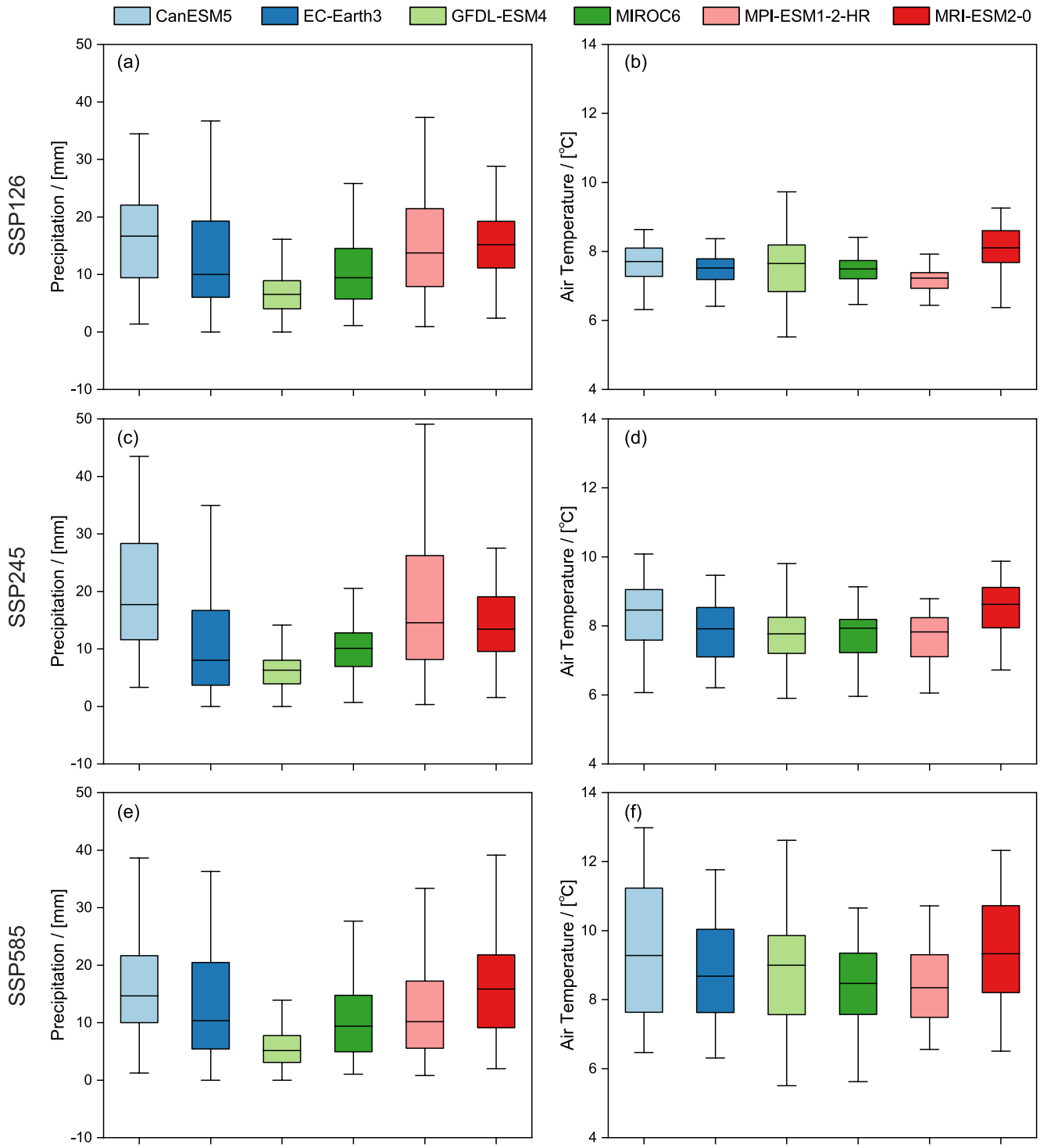

Figure 10. Total precipitation (left column) during winter (i.e., December–February in the following year) and mean air temperature (right column) during summer (i.e., June–August) from six Coupled Model Intercomparison Project Phase 6 Global Climate Models under three Shared Socioeconomic Pathway scenarios from 2018 to 2100.

Nyainqentanglha Mountain in Rounce et al. (2020). Hock et al. (2019) systematically compared global-scale glacier mass change projections from six published global glacier models as part of the Glacier Model Intercomparison Project (GlacierMIP). Glacier mass projections vary among different global glacier models, and relative volume loss (the average of all model runs ±1 standard deviation) for South Asia (East) by 2100 is 77% ± 19%

for RCP8.5. Marzeion et al. (2020) presented glacier mass and area change projections for the 21st century based on 11 glacier models. Results showed that the relative volume loss (the average of all model runs ±1 standard deviation) for South Asia (East) by 2100 is 83% ± 17% for RCP8.5. Hence, glacier mass change projections for the same region also vary in different studies, but both Hock et al. (2019) and Marzeion et al. (2020) found that South Asia (East) is likely to experience significant mass loss by 2100 and that glaciers over this region may even disappear under the RCP 8.5 scenario. Rounce et al. (2020) projected glacier mass changes for HMA by the end of this century, and indicated that Nyainqentanglha would lose glacier mass of 88% ± 6% by 2100 under RCP8.5. These results are consistent with our findings, that is, a representative glacier of South Asia (East) and Nyainqentanglha (the Parlung No. 94 Glacier) would experience a mass loss of 98% ± 3% from 2018 to 2100 under the SSP585 scenario, and would almost disappear by the end of the century.

As for the Dongkemadi Glacier located in the hinterland of the TP, the range of Central Asia in Hock et al. (2019) and Marzeion et al. (2020) is too large and the climate varies substantially across different sites. Hence, we compared the glacier change projections of the Dongkemadi Glacier with those of Tanggula Shan in Rounce et al. (2020). Results from Rounce et al. (2020) indicated that Tanggula Shan is likely to lose glacier mass of 95% ± 5% by 2100 under RCP8.5, which is consistent with our projection that the Dongkemadi Glacier would experience a mass loss of 97% ± 4% from 2018 to 2100 under the SSP585 scenario. Gao et al. (2021) assessed the impact of future climate change on glacier response and its hydrological effects for the same region as our study (the Dongkemadi Glacier). Results showed that glacier mass is expected to decrease by 74% and 92% by 2100 for RCP2.6 and RCP8.5, respectively. The glacier runoff is projected to increase and reach peak water around 2060 to 2085. Both the projection of glacier mass loss and the peak water timing of glacier runoff are consistent with our results. Overall, the projection of glacier changes in response to climate change in our study is consistent with previous studies, and differences inevitably exist because the study region, glacier model and GCMs are not the same across our study and previous studies. Further analysis of different factors on uncertainty of glacier change projection can be found in Text S3 in Supporting Information S1 and Figure S7 in Supporting Information S2.

6. Conclusion

Glaciers in alpine regions play an important role in providing water supply for the populations and ecosystems in downstream regions. Thus, accurate projection of glacier response to climate change is essential for water resource management and risk prevention. In this study, we developed a hybrid modeling approach by coupling an empirical glacier evolution model (Δh-parameterization) with a temperature-index snow and ice melt model (TSI), and applied the TSI-Δh model to the Parlung No. 94 Glacier and the Dongkemadi Glacier, to improve our understanding of the future evolution of different types of glaciers in response to climate change. Results from the glacier mass balance simulations indicate that the continental glacier (Xiao Dongkemadi Glacier) has a lower balance amplitude than the maritime glacier (the Parlung No. 94 Glacier). The net mass balance rate is small or even positive in some years for the continental glacier, while the Parlung No. 94 Glacier has a larger net mass balance rate (negative). According to the projections using the TSI-Δh model, the Parlung No. 94 Glacier and the Dongkemadi Glacier are expected to recede continuously, even under the optimistic climate scenario (SSP126). They are likely to melt away almost completely by 2100 under the highest emission scenario (SSP585).

Specifically, the Parlung No. 94 Glacier is projected to experience a mass loss of 80% ± 14% (SSP126), 88% ± 8% (SSP245), and 98% ± 3% (SSP585) by 2100, and the Dongkemadi Glacier to experience a mass loss of 75% ± 23% (SSP126), 88% ± 12% (SSP245), and 97% ± 4% (SSP585). The projected years for the halving of the Dongkemadi Glacier's volume (area) relative to 2018 are about 5–11 (14) years later than the Parlung No. 94 Glacier due to the lower rate of retreat of continental glaciers. The glacier runoff projections indicate that peak glacier runoff occurs later and is larger for higher emission scenarios and for the continental glacier than the maritime glacier. Peak water of the Parlung No. 94 Glacier is expected to occur by the mid-21st-century under the highest emission scenario, while the peak water year for the Dongkemadi Glacier is 2072. The timing of peak water is controlled mostly by glacier meltwater, which is the largest contributor of glacier runoff. The magnitude of glacier runoff is affected by glacier melt together with precipitation, and a later timing of peak water results in a larger magnitude due to more precipitation.

Overall, the results of this study show that the hybrid modeling approach performs well and discrepancies exist in the projections of future glacier evolution in response to climate change for the maritime and continental glaciers.

With the increasing availability of regional/global glacier data sets such as geodetic mass balance data sets, the proposed approach can be applied to more glaciers to examine their projected response to climate change.

Data Availability Statement

ERA5 forcing data (Boogaard et al., 2020) are available at https://cds.climate.copernicus.eu/cdsapp#!/dataset/10.24381/cds.6c68c9bb?tab=overview. GCM CanESM5 data of CMIP6 (Swart et al., 2019) are available at http://doi.org/10.22033/ESGF/CMIP6.3610. GCM EC-Earth3 data of CMIP6 (EC-Earth Consortium, 2019) are available at http://doi.org/10.22033/ESGF/CMIP6.4700. GCM GFDL-ESM4 data of CMIP6 (Krasting et al., 2018) are available at http://doi.org/10.22033/ESGF/CMIP6.8597. GCM MIROC6 data of CMIP6 (Tatebe and Watanabe., 2018) are available at http://doi.org/10.22033/ESGF/CMIP6.5603. GCM MPI-ESM1-2-HR data of CMIP6 (Jungclaus et al., 2019) are available at http://doi.org/10.22033/ESGF/CMIP6.6594. GCM MRI-ESM2-0 data of CMIP6 (Yukimoto et al., 2019) are available at http://doi.org/10.22033/ESGF/CMIP6.6842. NASADEM Merged DEM Global 1 arc s V001 (NASA JPL, 2020) is available at https://doi.org/10.5067/MEaSUREs/NASADEM/NASADEM_HGT.001. Glacier mass balance observations (WGMS, 2022) are available at https://doi.org/10.5904/wgms-fog-2022-09. Estimated glacier ice thickness (Farinotti et al., 2019b) is available at https://doi.org/10.3929/ethz-b-000315707. RGI 6.0 glacier mask (RGI Consortium, 2017) can be accessed at https://doi.org/10.7265/4m1f-gd79. Additional data (Han et al., 2023) are available at the Zenodo data repository (https://doi.org/10.5281/zenodo.7732689).

Acknowledgments
This study was supported by the Second Tibetan Plateau Scientific Expedition and Research (STEP) program (2019QZKK0105) and the National Natural Science Foundation of China (Grants 92047301 and 92047203). LJS is supported by the UK Research and Innovation (MR/V022008/1). Comments from reviewers and editors were valuable in improving this study and highly appreciated.

References

Bach, E., Radić, V., & Schoof, C. (2018). How sensitive are mountain glaciers to climate change? Insights from a block model. *Journal of Glaciology*, *64*(244), 247–258. https://doi.org/10.1017/jog.2018.15

Bahr, D. B., Meier, M. F., & Peckham, S. D. (1997). The physical basis of glacier volume-area scaling. *Journal of Geophysical Research*, *102*(B9), 20355–20362. https://doi.org/10.1029/97jb01696

Bamber, J. L., Westaway, R. M., Marzeion, B., & Wouters, B. (2018). The land ice contribution to sea level during the satellite era. *Environmental Research Letters*, *13*(6), 063008. https://doi.org/10.1088/1748-9326/aac2f0

Bhutiyani, M. R., Kale, V. S., & Pawar, N. (2010). Climate change and the precipitation variations in the northwestern Himalaya: 1866–2006. *International Journal of Climatology: A Journal of the Royal Meteorological Society*, *30*(4), 535–548. https://doi.org/10.1002/joc.1920

Biemans, H., Siderius, C., Lutz, A. F., Nepal, S., Ahmad, B., Hassan, T., et al. (2019). Importance of snow and glacier meltwater for agriculture on the Indo-Gangetic Plain. *Nature Sustainability*, *2*(7), 594–601. https://doi.org/10.1038/s41893-019-0305-3

Bliss, A., Hock, R., & Radić, V. (2014). Global response of glacier runoff to twenty-first century climate change. *Journal of Geophysical Research: Earth Surface*, *119*(4), 717–730. https://doi.org/10.1002/2013jf002931

Blöschl, G., Kirnbauer, R., & Gutknecht, D. (1991). Distributed snowmelt simulations in an alpine catchment: 1. Model evaluation on the basis of snow cover patterns. *Water Resources Research*, *27*(12), 3171–3179. https://doi.org/10.1029/91wr02250

Boogaard, H., van der Gerald, G., & de Allard, W. (2020). Agrometeorological indicators from 1979 to present derived from reanalysis [Dataset]. Copernicus Climate Change Service (C3S) Climate Data Store (CDS). https://doi.org/10.24381/cds.6c68c9bb

Braithwaite, R. J., & Hughes, P. D. (2020). Regional geography of Glacier Mass balance variability over seven decades 1946–2015. *Frontiers of Earth Science*, *8*, 302. https://doi.org/10.3389/feart.2020.00302

Brun, F., Berthier, E., Wagnon, P., Kääb, A., & Treichler, D. (2017). A spatially resolved estimate of High Mountain Asia glacier mass balances from 2000 to 2016. *Nature Geoscience*, *10*(9), 668–673. https://doi.org/10.1038/ngeo2999

Cannon, A. J., Sobie, S. R., & Murdock, T. Q. (2015). Bias correction of GCM precipitation by quantile mapping: How well do methods preserve changes in quantiles and extremes? *Journal of Climate*, *28*(17), 6938–6959. https://doi.org/10.1175/jcli-d-14-00754.1

Chen, X., Long, D., Hong, Y., Zeng, C., & Yan, D. (2017). Improved modeling of snow and glacier melting by a progressive two-stage calibration strategy with GRACE and multisource data: How snow and glacier meltwater contributes to the runoff of the Upper Brahmaputra River basin? *Water Resources Research*, *53*(3), 2431–2466. https://doi.org/10.1002/2016wr019656

Consortium, R. (2017). Randolph Glacier inventory–A dataset of global glacier outlines: Version 6.0: Technical Report, global land ice measurements from space.

Cook, B., Mankin, J., Marvel, K., Williams, A., Smerdon, J., & Anchukaitis, K. (2020). Twenty-first century drought projections in the CMIP6 forcing scenarios. *Earth's Future*, *8*(6), e2019EF001461. https://doi.org/10.1029/2019ef001461

Deb, K., Pratap, A., Agarwal, S., & Meyarivan, T. (2002). A fast and elitist multiobjective genetic algorithm: NSGA-II. *IEEE Transactions on Evolutionary Computation*, *6*(2), 182–197. https://doi.org/10.1109/4235.996017

EC-Earth Consortium (EC-Earth). (2019). EC-Earth-Consortium EC-Earth3 model output prepared for CMIP6 CMIP historical [Dataset]. Earth System Grid Federation. https://doi.org/10.22033/ESGF/CMIP6.4700

Edwards, T. L., Nowicki, S., Marzeion, B., Hock, R., Goelzer, H., Seroussi, H., et al. (2021). Projected land ice contributions to twenty-first-century sea level rise. *Nature*, *593*(7857), 74–82. https://doi.org/10.1038/s41586-021-03302-y

Eis, J., van der Laan, L., Maussion, F., & Marzeion, B. (2021). Reconstruction of past glacier changes with an ice-flow glacier model: Proof of concept and validation. *Frontiers of Earth Science*, *9*, 595755. https://doi.org/10.3389/feart.2021.595755

Engelhardt, M., Schuler, T. V., & Andreassen, L. M. (2013). Glacier mass balance of Norway 1961–2010 calculated by a temperature-index model. *Annals of Glaciology*, *54*(63), 32–40. https://doi.org/10.3189/2013aog63a245

Engelhardt, M., Schuler, T. V., & Andreassen, L. M. (2014). Contribution of snow and glacier melt to discharge for highly glacierised catchments in Norway. *Hydrology and Earth System Sciences*, *18*(2), 511–523. https://doi.org/10.5194/hess-18-511-2014

Farinotti, D., Huss, M., Fürst, J. J., Landmann, J., Machguth, H., Maussion, F., & Pandit, A. (2019a). A consensus estimate for the ice thickness distribution of all glaciers on Earth. *Nature Geoscience*, *12*(3), 168–173. https://doi.org/10.1038/s41561-019-0300-3

Farinotti, D., Huss, M., Fürst, J. J., Landmann, J., Machguth, H., Maussion, F., & Pandit, A. (2019b). Supplementary data to: A consensus estimate for the ice thickness distribution of all glaciers on Earth [Dataset]. ETH Zurich. https://doi.org/10.3929/ethz-b-000315707
Fontaine, T., Cruickshank, T., Arnold, J., & Hotchkiss, R. (2002). Development of a snowfall–snowmelt routine for mountainous terrain for the soil water assessment tool (SWAT). *Journal of Hydrology*, *262*(1–4), 209–223. https://doi.org/10.1016/s0022-1694(02)00029-x
Gao, H., Feng, Z., Zhang, T., Wang, Y., He, X., Li, H., et al. (2021). Assessing glacier retreat and its impact on water resources in a headwater of Yangtze River based on CMIP6 projections. *Science of the Total Environment*, *765*, 142774. https://doi.org/10.1016/j.scitotenv.2020.142774
Gao, H., He, X., Ye, B., & Pu, J. (2012). Modeling the runoff and glacier mass balance in a small watershed on the Central Tibetan Plateau, China, from 1955 to 2008. *Hydrological Processes*, *26*(11), 1593–1603. https://doi.org/10.1002/hyp.8256
Gardner, A. S., Moholdt, G., Cogley, J. G., Wouters, B., Arendt, A. A., Wahr, J., et al. (2013). A reconciled estimate of glacier contributions to sea level rise: 2003 to 2009. *Science*, *340*(6134), 852–857. https://doi.org/10.1126/science.1234532
Gidden, M. J., Riahi, K., Smith, S. J., Fujimori, S., Luderer, G., Kriegler, E., et al. (2019). Global emissions pathways under different socioeconomic scenarios for use in CMIP6: A dataset of harmonized emissions trajectories through the end of the century. *Geoscientific Model Development*, *12*(4), 1443–1475. https://doi.org/10.5194/gmd-12-1443-2019
Haeberli, W., & Beniston, M. (1998). Climate change and its impacts on glaciers and permafrost in the Alps. *Ambio*, *27*, 258–265.
Haeberli, W., Maisch, M., & Paul, F. (2002). Mountain glaciers in global climate-related observation networks. *World Meteorological Organization Bulletin*, *51*(1), 18–25.
Hagg, W., Hoelzle, M., Wagner, S., Mayr, E., & Klose, Z. (2013). Glacier and runoff changes in the Rukhk catchment, upper Amu-Darya basin until 2050. *Global and Planetary Change*, *110*, 62–73. https://doi.org/10.1016/j.gloplacha.2013.05.005
Han, P., Long, D., Han, Z., Du, M., Dai, L., & Hao, X. (2019). Improved understanding of snowmelt runoff from the headwaters of China's Yangtze River using remotely sensed snow products and hydrological modeling. *Remote Sensing of Environment*, *224*, 44–59. https://doi.org/10.1016/j.rse.2019.01.041
Han, P., Long, D., Li, X., Huang, Q., Dai, L., & Sun, Z. (2021). A dual state-parameter updating scheme using the particle filter and high-spatial-resolution remotely sensed snow depths to improve snow simulation. *Journal of Hydrology*, *594*, 125979. https://doi.org/10.1016/j.jhydrol.2021.125979
Han, P., Long, D., Zhao, F., & Slater, L. (2023). High spatial resolution satellite images for glacier outlines [Dataset]. Zenodo. https://doi.org/10.5281/zenodo.7732689
Hersbach, H., Bell, B., Berrisford, P., Hirahara, S., Horányi, A., Muñoz-Sabater, J., et al. (2020). The ERA5 global reanalysis. *Quarterly Journal of the Royal Meteorological Society*, *146*(730), 1999–2049. https://doi.org/10.1002/qj.3803
Hock, R. (2003). Temperature index melt modelling in mountain areas. *Journal of Hydrology*, *282*(1–4), 104–115. https://doi.org/10.1016/s0022-1694(03)00257-9
Hock, R., Bliss, A., Marzeion, B., Giesen, R. H., Hirabayashi, Y., Huss, M., et al. (2019). GlacierMIP—A model intercomparison of global-scale glacier mass-balance models and projections. *Journal of Glaciology*, *65*(251), 453–467. https://doi.org/10.1017/jog.2019.22
Hofer, S., Lang, C., Amory, C., Kittel, C., Delhasse, A., Tedstone, A., & Fettweis, X. (2020). Greater Greenland Ice Sheet contribution to global sea level rise in CMIP6. *Nature Communications*, *11*(1), 1–11. https://doi.org/10.1038/s41467-020-20011-8
Hong, Z., Han, Z., Li, X., Long, D., Tang, G., & Wang, J. (2021). Generation of an improved precipitation dataset from multisource information over the Tibetan Plateau. *Journal of Hydrometeorology*, *22*(5), 1275–1295. https://doi.org/10.1175/jhm-d-20-0252.1
Hugonnet, R., McNabb, R., Berthier, E., Menounos, B., Nuth, C., Girod, L., et al. (2021). Accelerated global glacier mass loss in the early twenty-first century. *Nature*, *592*(7856), 726–731. https://doi.org/10.1038/s41586-021-03436-z
Huss, M., Bauder, A., Funk, M., & Hock, R. (2008). Determination of the seasonal mass balance of four Alpine glaciers since 1865. *Journal of Geophysical Research*, *113*(F1), F01015. https://doi.org/10.1029/2007jf000803
Huss, M., & Hock, R. (2015). A new model for global glacier change and sea-level rise. *Frontiers of Earth Science*, *3*, 54. https://doi.org/10.3389/feart.2015.00054
Huss, M., & Hock, R. (2018). Global-scale hydrological response to future glacier mass loss. *Nature Climate Change*, *8*(2), 135–140. https://doi.org/10.1038/s41558-017-0049-x
Huss, M., Jouvet, G., Farinotti, D., & Bauder, A. (2010). Future high-mountain hydrology: A new parameterization of glacier retreat. *Hydrology and Earth System Sciences*, *14*(5), 815–829. https://doi.org/10.5194/hess-14-815-2010
Immerzeel, W. W., Lutz, A., Andrade, M., Bahl, A., Biemans, H., Bolch, T., et al. (2020). Importance and vulnerability of the world's water towers. *Nature*, *577*(7790), 364–369. https://doi.org/10.1038/s41586-019-1822-y
Jiang, Y., Yang, K., Shao, C., Zhou, X., Zhao, L., Chen, Y., & Wu, H. (2021). A downscaling approach for constructing high-resolution precipitation dataset over the Tibetan Plateau from ERA5 reanalysis. *Atmospheric Research*, *256*, 105574. https://doi.org/10.1016/j.atmosres.2021.105574
Jungclaus, J., Bittner, M., Wieners, K. H., Wachsmann, F., Schupfner, M., Legutke, S., et al. (2019). MPI-M MPI-ESM1.2-HR model output prepared for CMIP6 CMIP historical [Dataset]. Earth System Grid Federation. https://doi.org/10.22033/ESGF/CMIP6.6594
Kochtitzky, W., & Copland, L. (2022). Retreat of Northern Hemisphere marine-terminating Glaciers, 2000–2020. *Geophysical Research Letters*, *49*(3), e2021GL096501. https://doi.org/10.1029/2021gl096501
Konz, M., & Seibert, J. (2010). On the value of glacier mass balances for hydrological model calibration. *Journal of Hydrology*, *385*(1–4), 238–246. https://doi.org/10.1016/j.jhydrol.2010.02.025
Kraaijenbrink, P. D., Bierkens, M., Lutz, A., & Immerzeel, W. (2017). Impact of a global temperature rise of 1.5 degrees Celsius on Asia's glaciers. *Nature*, *549*(7671), 257–260. https://doi.org/10.1038/nature23878
Krasting, J. P., John, J. G., Blanton, C., McHugh, C., Nikonov, S., Radhakrishnan, A., et al. (2018). NOAA-GFDL GFDL-ESM4 model output prepared for CMIP6 CMIP historical [Dataset]. Earth System Grid Federation. https://doi.org/10.22033/ESGF/CMIP6.8597
Kuczera, G., & Parent, E. (1998). Monte Carlo assessment of parameter uncertainty in conceptual catchment models: The metropolis algorithm. *Journal of Hydrology*, *211*(1–4), 69–85. https://doi.org/10.1016/s0022-1694(98)00198-x
Kulkarni, A. V. (1992). Mass balance of Himalayan glaciers using AAR and ELA methods. *Journal of Glaciology*, *38*(128), 101–104. https://doi.org/10.3189/s0022143000009631
Kulkarni, A. V., Rathore, B., & Alex, S. (2004). Monitoring of glacial mass balance in the Baspa basin using accumulation area ratio method. *Current Science*, 185–190.
Li, X., Long, D., Scanlon, B. R., Mann, M. E., Li, X., Tian, F., et al. (2022). Climate change threatens terrestrial water storage over the Tibetan Plateau. *Nature Climate Change*, *12*(9), 801–807. https://doi.org/10.1038/s41558-022-01443-0
Liang, L., Cuo, L., & Liu, Q. (2018). The energy and mass balance of a continental glacier: Dongkemadi Glacier in central Tibetan Plateau. *Scientific Reports*, *8*(1), 12788. https://doi.org/10.1038/s41598-018-31228-5
Marzeion, B., Hock, R., Anderson, B., Bliss, A., Champollion, N., Fujita, K., et al. (2020). Partitioning the uncertainty of ensemble projections of global glacier mass change. *Earth's Future*, *8*(7), e2019EF001470. https://doi.org/10.1029/2019ef001470

Marzeion, B., Jarosch, A. H., & Hofer, M. (2012). Past and future sea-level change from the surface mass balance of glaciers. *The Cryosphere*, *6*(6), 1295–1322. https://doi.org/10.5194/tc-6-1295-2012
Maurer, J. M., Schaefer, J. M., Rupper, S., & Corley, A. (2019). Acceleration of ice loss across the Himalayas over the past 40 years. *Science Advances*, *5*(6), eaav7266. https://doi.org/10.1126/sciadv.aav7266
Maussion, F., Butenko, A., Champollion, N., Dusch, M., Eis, J., Fourteau, K., et al. (2019). The open Global Glacier Model (OGGM) v1.1. *Geoscientific Model Development*, *12*(3), 909–931. https://doi.org/10.5194/gmd-12-909-2019
Millan, R., Mouginot, J., Rabatel, A., & Morlighem, M. (2022). Ice velocity and thickness of the world's glaciers. *Nature Geoscience*, *15*(2), 124–129. https://doi.org/10.1038/s41561-021-00885-z
Moholdt, G., Nuth, C., Hagen, J. O., & Kohler, J. (2010). Recent elevation changes of Svalbard glaciers derived from ICESat laser altimetry. *Remote Sensing of Environment*, *114*(11), 2756–2767. https://doi.org/10.1016/j.rse.2010.06.008
NASA, J. P. L. (2020). NASADEM Merged DEM Global 1 arc second V001 [Dataset]. NASA EOSDIS Land Processes DAAC. https://doi.org/10.5067/MEaSUREs/NASADEM/NASADEM_HGT.001
Nolin, A. W., Phillippe, J., Jefferson, A., & Lewis, S. L. (2010). Present-day and future contributions of glacier runoff to summertime flows in a Pacific Northwest watershed: Implications for water resources. *Water Resources Research*, *46*(12), W12509. https://doi.org/10.1029/2009wr008968
Ohmura, A. (2001). Physical basis for the temperature-based melt-index method. *Journal of Applied Meteorology*, *40*(4), 753–761. https://doi.org/10.1175/1520-0450(2001)040<0753:pbfttb>2.0.co;2
Omani, N., Srinivasan, R., Smith, P. K., & Karthikeyan, R. (2017). Glacier mass balance simulation using SWAT distributed snow algorithm. *Hydrological Sciences Journal*, *62*(4), 546–560. https://doi.org/10.1080/02626667.2016.1162907
O'Neel, S., Hood, E., Arendt, A., & Sass, L. (2014). Assessing streamflow sensitivity to variations in glacier mass balance. *Climatic Change*, *123*(2), 329–341. https://doi.org/10.1007/s10584-013-1042-7
O'Neill, B. C., Tebaldi, C., Vuuren, D. P. V., Eyring, V., Friedlingstein, P., Hurtt, G., et al. (2016). The scenario model intercomparison project (ScenarioMIP) for CMIP6. *Geoscientific Model Development*, *9*(9), 3461–3482. https://doi.org/10.5194/gmd-9-3461-2016
Pepin, N., Bradley, R. S., Diaz, H., Baraër, M., Caceres, E., Forsythe, N., et al. (2015). Elevation-dependent warming in mountain regions of the world. *Nature Climate Change*, *5*(5), 424–430. https://doi.org/10.1038/nclimate2563
Pritchard, H. D. (2019). Asia's shrinking glaciers protect large populations from drought stress. *Nature*, *569*(7758), 649–654. https://doi.org/10.1038/s41586-019-1240-1
Pu, J., Yao, T., Yang, M., Tian, L., Wang, N., Ageta, Y., & Fujita, K. (2008). Rapid decrease of mass balance observed in the Xiao (Lesser) Dongkemadi Glacier, in the central Tibetan plateau. *Hydrological Processes: International Journal*, *22*(16), 2953–2958. https://doi.org/10.1002/hyp.6865
Radić, V., & Hock, R. (2006). Modeling future glacier mass balance and volume changes using ERA-40 reanalysis and climate models: A sensitivity study at Storglaciären, Sweden. *Journal of Geophysical Research*, *111*(F3), F03003. https://doi.org/10.1029/2005jf000440
Rahman, K., Maringanti, C., Beniston, M., Widmer, F., Abbaspour, K., & Lehmann, A. (2013). Streamflow modeling in a highly managed mountainous glacier watershed using SWAT: The upper Rhone river watershed case in Switzerland. *Water Resources Management*, *27*(2), 323–339. https://doi.org/10.1007/s11269-012-0188-9
Reveillet, M., Vincent, C., Six, D., & Rabatel, A. (2017). Which empirical model is best suited to simulate glacier mass balances? *Journal of Glaciology*, *63*(237), 39–54. https://doi.org/10.1017/jog.2016.110
RGI Consortium. (2017). Randolph Glacier inventory—A dataset of global glacier outlines, version 6 [Dataset]. Boulder, Colorado USA. National Snow and Ice Data Center. https://doi.org/10.7265/4m1f-gd79
Rounce, D. R., Hock, R., & Shean, D. E. (2020). Glacier mass change in High Mountain Asia through 2100 using the open-source python glacier evolution model (PyGEM). *Frontiers of Earth Science*, *7*, 331. https://doi.org/10.3389/feart.2019.00331
Sagredo, E. A., Rupper, S., & Lowell, T. V. (2014). Sensitivities of the equilibrium line altitude to temperature and precipitation changes along the Andes. *Quaternary Research*, *81*(2), 355–366. https://doi.org/10.1016/j.yqres.2014.01.008
Schaefli, B., Hingray, B., & Musy, A. (2007). Climate change and hydropower production in the Swiss Alps: Quantification of potential impacts and related modelling uncertainties. *Hydrology and Earth System Sciences*, *11*(3), 1191–1205. https://doi.org/10.5194/hess-11-1191-2007
Schuler, T. V., Loe, E., Taurisano, A., Eiken, T., Hagen, J. O., & Kohler, J. (2007). Calibrating a surface mass-balance model for Austfonna ice cap, Svalbard. *Annals of Glaciology*, *46*, 241–248. https://doi.org/10.3189/172756407782871783
Seibert, J., Vis, M. J., Kohn, I., Weiler, M., & Stahl, K. (2018). Representing glacier geometry changes in a semi-distributed hydrological model. *Hydrology and Earth System Sciences*, *22*(4), 2211–2224. https://doi.org/10.5194/hess-22-2211-2018
Shean, D. E., Bhushan, S., Montesano, P., Rounce, D. R., Arendt, A., & Osmanoglu, B. (2020). A systematic, regional assessment of high mountain Asia glacier mass balance. *Frontiers of Earth Science*, *7*, 363. https://doi.org/10.3389/feart.2019.00363
Shi, Y., Liu, C., & Wang, Z. (2008). *Concise Glacier inventory of China*. Shanghai Popular Science Press.
Stahl, K., Moore, R., Shea, J., Hutchinson, D., & Cannon, A. (2008). Coupled modelling of glacier and streamflow response to future climate scenarios. *Water Resources Research*, *44*(2), WR005956. https://doi.org/10.1029/2007wr005956
Swart, N. C., Cole, J. N., Kharin, V. V., Lazare, M., Scinocca, J. F., Gillett, N. P., et al. (2019). CCCma CanESM5 model output prepared for CMIP6 CMIP historical [Dataset]. Earth System Grid Federation. https://doi.org/10.22033/ESGF/CMIP6.3610
Tang, J., Cheng, H., & Liu, L. (2014). Assessing the recent droughts in Southwestern China using satellite gravimetry. *Water Resources Research*, *50*(4), 3030–3038. https://doi.org/10.1002/2013wr014656
Tatebe, H., & Watanabe, M. (2018). MIROC MIROC6 model output prepared for CMIP6 CMIP historical [Dataset]. Earth System Grid Federation. https://doi.org/10.22033/ESGF/CMIP6.5603
Tokarska, K. B., Stolpe, M. B., Sippel, S., Fischer, E. M., Smith, C. J., Lehner, F., & Knutti, R. (2020). Past warming trend constrains future warming in CMIP6 models. *Science Advances*, *6*(12), eaaz9549. https://doi.org/10.1126/sciadv.aaz9549
Viviroli, D., Dürr, H. H., Messerli, B., Meybeck, M., & Weingartner, R. (2007). Mountains of the world, water towers for humanity: Typology, mapping, and global significance. *Water Resources Research*, *43*(7), W07447. https://doi.org/10.1029/2006wr005653
Vuille, M., Francou, B., Wagnon, P., Juen, I., Kaser, G., Mark, B. G., & Bradley, R. S. (2008). Climate change and tropical Andean glaciers: Past, present and future. *Earth-Science Reviews*, *89*(3–4), 79–96. https://doi.org/10.1016/j.earscirev.2008.04.002
Wang, S. J. (2018). Spatiotemporal variability of temperature trends on the southeast Tibetan Plateau, China. *International Journal of Climatology*, *38*(4), 1953–1963. https://doi.org/10.1002/joc.5308
Wang, T., Zhao, Y., Xu, C., Ciais, P., Liu, D., Yang, H., et al. (2021). Atmospheric dynamic constraints on Tibetan Plateau freshwater under Paris climate targets. *Nature Climate Change*, *11*(3), 219–225. https://doi.org/10.1038/s41558-020-00974-8
Wang, W., Yao, T., & Yang, X. (2011). Variations of glacial lakes and glaciers in the Boshula mountain range, southeast Tibet, from the 1970s to 2009. *Annals of Glaciology*, *52*(58), 9–17. https://doi.org/10.3189/172756411797252347

WGMS. (2022). Fluctuations of Glaciers database [Dataset]. World Glacier Monitoring Service (WGMS). Zurich, Switzerland. https://doi.org/10.5904/wgms-fog-2022-09

Wijngaard, R. R., Steiner, J. F., Kraaijenbrink, P. D. A., Klug, C., Adhikari, S., Banerjee, A., et al. (2019). Modeling the response of the langtang glacier and the hintereisferner to a changing climate since the little ice age. *Frontiers of Earth Science*, *7*, 143. https://doi.org/10.3389/feart.2019.00143

Xu, J., Grumbine, R. E., Shrestha, A., Eriksson, M., Yang, X., Wang, Y., & Wilkes, A. (2009). The melting Himalayas: Cascading effects of climate change on water, biodiversity, and livelihoods. *Conservation Biology*, *23*(3), 520–530. https://doi.org/10.1111/j.1523-1739.2009.01237.x

Xu, M., Yan, M., Kang, J., & Ren, J. (2012). Comparative studies of glacier mass balance and their climatic implications in Svalbard, Northern Scandinavia, and Southern Norway. *Environmental Earth Sciences*, *67*(5), 1407–1414. https://doi.org/10.1007/s12665-012-1585-3

Yang, W., Yao, T., Guo, X., Zhu, M., Li, S., & Kattel, D. B. (2013). Mass balance of a maritime glacier on the southeast Tibetan Plateau and its climatic sensitivity. *Journal of Geophysical Research: Atmospheres*, *118*(17), 9579–9594. https://doi.org/10.1002/jgrd.50760

Yang, W., Yao, T., Xu, B., Ma, L., Wang, Z., & Wan, M. (2010). Characteristics of recent temperate glacier fluctuations in the Parlung Zangbo River basin, southeast Tibetan Plateau. *Chinese Science Bulletin*, *55*(20), 2097–2102. https://doi.org/10.1007/s11434-010-3214-4

Yang, W., Yao, T., Xu, B., Wu, G., Ma, L., & Xin, X. (2008). Quick ice mass loss and abrupt retreat of the maritime glaciers in the Kangri Karpo Mountains, southeast Tibetan Plateau. *Chinese Science Bulletin*, *53*(16), 2547–2551. https://doi.org/10.1007/s11434-008-0288-3

Yao, T., Thompson, L., Yang, W., Yu, W., Gao, Y., Guo, X., et al. (2012). Different glacier status with atmospheric circulations in Tibetan Plateau and surroundings. *Nature Climate Change*, *2*(9), 663–667. https://doi.org/10.1038/nclimate1580

You, Q., Chen, D., Wu, F., Pepin, N., Cai, Z., Ahrens, B., et al. (2020). Elevation dependent warming over the Tibetan Plateau: Patterns, mechanisms and perspectives. *Earth-Science Reviews*, *210*, 103349. https://doi.org/10.1016/j.earscirev.2020.103349

Yukimoto, S., Kawai, H., Koshiro, T., Oshima, N., Yoshida, K., Urakawa, S., et al. (2019). MRI MRI-ESM2.0 model output prepared for CMIP6 CMIP historical [Dataset]. Earth System Grid Federation. https://doi.org/10.22033/ESGF/CMIP6.6842

Zekollari, H., Huss, M., Farinotti, D., & Lhermitte, S. (2022). Ice-dynamical glacier evolution modeling—A review. *Reviews of Geophysics*, *60*(2), e2021RG000754. https://doi.org/10.1029/2021rg000754

Zemp, M., Frey, H., Gärtner-Roer, I., Nussbaumer, S. U., Hoelzle, M., Paul, F., et al. (2015). Historically unprecedented global glacier decline in the early 21st century. *Journal of Glaciology*, *61*(228), 745–762. https://doi.org/10.3189/2015jog15j017

Zemp, M., Huss, M., Thibert, E., Eckert, N., McNabb, R., Huber, J., et al. (2019). Global glacier mass changes and their contributions to sea-level rise from 1961 to 2016. *Nature*, *568*(7752), 382–386. https://doi.org/10.1038/s41586-019-1071-0

Zhao, F., Long, D., Li, X., Huang, Q., & Han, P. (2022). Rapid glacier mass loss in the Southeastern Tibetan Plateau since the year 2000 from satellite observations. *Remote Sensing of Environment*, *270*, 112853. https://doi.org/10.1016/j.rse.2021.112853